



HAL
open science

Sulfates and Iron Oxides in Ophir Chasma, Mars, based on OMEGA and CRISM observations

Lorenz Wendt, Christoph Gross, Thomas Kneissl, Mariam Sowe, Jean-Philippe Combe, Laetitia Ledoit, Patrick C. Mcguire, Gerhard Neukum

► **To cite this version:**

Lorenz Wendt, Christoph Gross, Thomas Kneissl, Mariam Sowe, Jean-Philippe Combe, et al.. Sulfates and Iron Oxides in Ophir Chasma, Mars, based on OMEGA and CRISM observations. *Icarus*, 2011, 10.1016/j.icarus.2011.02.013 . hal-00743842

HAL Id: hal-00743842

<https://hal.science/hal-00743842>

Submitted on 21 Oct 2012

HAL is a multi-disciplinary open access archive for the deposit and dissemination of scientific research documents, whether they are published or not. The documents may come from teaching and research institutions in France or abroad, or from public or private research centers.

L'archive ouverte pluridisciplinaire **HAL**, est destinée au dépôt et à la diffusion de documents scientifiques de niveau recherche, publiés ou non, émanant des établissements d'enseignement et de recherche français ou étrangers, des laboratoires publics ou privés.

Accepted Manuscript

Sulfates and Iron Oxides in Ophir Chasma, Mars, based on OMEGA and CRISM observations

Lorenz Wendt, Christoph Gross, Thomas Kneissl, Mariam Sowe, Jean-Philippe Combe, Laetitia LeDeit, Patrick C. McGuire, Gerhard Neukum

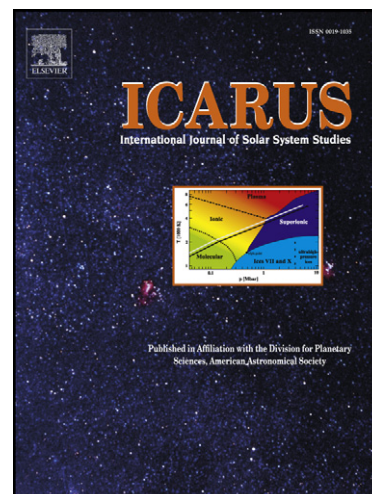
PII: S0019-1035(11)00071-6
DOI: [10.1016/j.icarus.2011.02.013](https://doi.org/10.1016/j.icarus.2011.02.013)
Reference: YICAR 9730

To appear in: *Icarus*

Received Date: 22 July 2010
Revised Date: 17 December 2010
Accepted Date: 15 February 2011

Please cite this article as: Wendt, L., Gross, C., Kneissl, T., Sowe, M., Combe, J-P., LeDeit, L., McGuire, P.C., Neukum, G., Sulfates and Iron Oxides in Ophir Chasma, Mars, based on OMEGA and CRISM observations, *Icarus* (2011), doi: [10.1016/j.icarus.2011.02.013](https://doi.org/10.1016/j.icarus.2011.02.013)

This is a PDF file of an unedited manuscript that has been accepted for publication. As a service to our customers we are providing this early version of the manuscript. The manuscript will undergo copyediting, typesetting, and review of the resulting proof before it is published in its final form. Please note that during the production process errors may be discovered which could affect the content, and all legal disclaimers that apply to the journal pertain.



1 Sulfates and Iron Oxides in Ophir Chasma, Mars, based on OMEGA and CRISM

2 observations

3

4 Lorenz Wendt^{a1}, Christoph Gross^{a2}, Thomas Kneissl^{a3}, Mariam Sowe^{a4}, Jean-Philippe

5 Combe^{b5}, Laetitia LeDeit^{c6}, Patrick C. McGuire^{a7}, Gerhard Neukum^{a8}

6

7 ^aInstitute of Geological Sciences, Freie Universität Berlin, Malteser Strasse 74-100,

8 12249 Berlin, Germany

9 ^bBear Fight Institute, P.O. Box 667, Winthrop WA 98862, USA

10 ^cGerman Aerospace Center (DLR), Institute of Planetary Research, Rutherfordstr. 2,

11 12489 Berlin, Germany

12

13 ¹lorenz.wendt@fu-berlin.de, Telephone: +493083870576, Fax: +493083870723

14 (corresponding author)

15 ²christoph.gross@fu-berlin.de

16 ³thomas.kneissl@fu-berlin.de

17 ⁴mariam.sowe@fu-berlin.de

18 ⁵jean-philippe_combe@bearfightinstitute.com

19 ⁶laetitia.ledeit@dlr.de

20 ⁷mcguire@geosci.uchicago.edu

21 ⁸gerhard.neukum@fu-berlin.de.

22 We investigate the sulfate and iron oxide deposits in Ophir Chasma, Mars, based on
23 short-wave infrared data from the Compact Reconnaissance Imaging Spectrometer for
24 Mars CRISM and from the Observatoire pour la Minéralogie, l'Eau, les Glaces et
25 l'Activité OMEGA. Sulfates are detected mainly in two locations. In the valley between
26 Ophir Mensa and the southern wall of Ophir Chasma, kieserite is found both within the
27 slope of Ophir Mensa, and superposed on the basaltic wall of the chasm. Here, kieserite is
28 unconformably overlain by polyhydrated sulfate deposits and iron oxides. Locally,
29 jarosite and unidentified phases with absorptions at 2.21 μm or 2.23 μm are detected,
30 which could be mixtures of jarosite and amorphous silica or other poorly crystalline
31 phases.

32 The second large sulfate-rich outcrop is found on the floor of the central valley. Although
33 the same minerals are found here, polyhydrated sulfates, kieserite, iron oxides, and
34 locally a possibly jarosite-bearing phase, this deposit is very distinct. It is not layered,
35 almost horizontal, and located at a much lower elevation of below -4250 m. Kieserite
36 superposes polyhydrated sulfate-rich deposits, and iron oxides form lags.

37 The facies of sulfate formation remains unclear, and could be different for the two
38 locations. A formation in a lake, playa or under a glacier is consistent with the
39 mineralogy of the central valley and its flat, low-lying topography. This is not
40 conceivable for the kieserite deposits observed south of Ophir Mensa. These deposits are
41 observed over several thousands of meters of elevation, which would require a standing
42 body of water several thousands of meters deep. This would have led to much more
43 pervasive sulfate deposits than observed. These deposits are therefore more consistent
44 with evaporation of groundwater infiltrating into previously sulfate-free light-toned

45 deposits. The overlying polyhydrated sulfates and other mineral phases are observed in
46 outcrops on ridges along the slopes of the southern chasm wall, which are too exposed to
47 be reached by groundwater. Here, a water supply from the atmosphere by rain, snow, fog
48 or frost is more conceivable.

49

50 Keywords: Mars, Surface, Spectroscopy

51

52 [SUGGESTED RUNNING TITLE

53 Sulfates and Iron Oxides in Ophir Chasma, Mars

54

ACCEPTED MANUSCRIPT

55 **1 Introduction**

56 The Light-Toned Deposits [LTD] or Interior Layered Deposits [ILD] (Lucchitta *et al.*, 1992)
57 within the chasmata of Valles Marineris are some of the most intensely studied geological
58 features on Mars. Many theories for their formation have been put forward, including subaerial
59 fluvial deposition or volcanism (Lucchitta *et al.*, 1992), accumulation of eolian dust or sand
60 (Peterson, 1981), evaporite precipitation in lakes (McKay and Nedell, 1988) or from
61 groundwater (Murchie *et al.*, 2009a), subaqueous (Nedell *et al.*, 1987) or sub-ice volcanism
62 (Chapman and Tanaka, 2001), or the formation as spring deposits (Rossi *et al.*, 2008), but a
63 conclusive theory combining all implications suggested by the composition, structure and
64 stratigraphic position of these deposits is still missing. A detailed discussion of the shortcomings
65 of each of the formation theories is provided by Lucchitta, 2009a; 2009b. One major constraint
66 on these theories is the role of liquid water, evidenced by the presence of ferric oxides and
67 sulfates, which are the subject of this study.

68 The mineralogy of the LTD's has been studied on a regional scale by Gendrin *et al.*, 2005 and
69 Mangold *et al.*, 2007, based on short-wave infrared (SWIR) data from the Observatoire pour la
70 Minéralogie, l'Eau, les Glaces et l'Activité OMEGA (Bibring *et al.*, 2004), and by Weitz *et al.*,
71 2008, based on thermal infrared data from the Thermal Emission Spectrometer TES (Christensen
72 *et al.*, 1992). A comparative study on the geological context of the individual outcrops of
73 aqueous minerals in Valles Marineris by Chojnacki and Hynek, 2008, showed that the LTDs are
74 much more diverse than previously thought, which makes a single formation process explaining
75 all depositions by the same mechanism less likely, and which raises the need for individual,
76 detailed mineralogic and geologic studies for each of the basins of Valles Marineris. In this
77 paper, we analyze SWIR data from OMEGA and the Compact Reconnaissance Imaging

78 Spectrometer for Mars CRISM (Murchie *et al.*, 2007) in combination with multispectral
79 imagery, digital elevation models and stereo images from the High Resolution Stereo Camera
80 HRSC (Neukum and Jaumann, 2004), and panchromatic images from HRSC, the Context Imager
81 CTX (Malin *et al.*, 2007) and the High Resolution Imaging Science Experiment HiRISE
82 (McEwen *et al.*, 2007) acquired over Ophir Chasma in order to understand the mineralogy and
83 local stratigraphy and layering characteristics of the water-related minerals found here, mainly
84 sulfates and iron oxides. Similar studies on neighboring chasmata include the work of Mangold
85 *et al.*, 2008, and Murchie *et al.*, 2009a, on West Candor Chasma, Le Deit *et al.*, 2008, on East
86 Candor Chasma, and Roach *et al.*, 2010b, on Ius Chasma.

87

88 [INSERT FIGURE 1 HERE]

89

90 Ophir Chasma is the northernmost depression of central Valles Marineris. It extends
91 approximately 270 km in East-West direction and 90 km in North-South direction (Fig. 1). The
92 floor of the chasma lies at elevations between 4200 and 4800 m below datum, its rim is at
93 elevations between 3400 and 4500 m above datum. Most of the western part of Ophir Chasma is
94 covered by a mound of LTDs, Ophir Mensa, which rises up to an elevation of 3200 m above
95 datum. This results in a total thickness of (at least) 7-8 km of deposits, assuming that the floor
96 below Ophir Mensa is approximately horizontal at an elevation close to the deepest points of the
97 chasm. Ophir Mensa is surrounded on all sides by depressions, which separate these deposits
98 from the chasm walls. For convenience, we informally named the depression to the north as the
99 "northern moat", the depression to the south as "mineral bowl", following Chojnacki and Hynek,

100 2008, and the depression to the east as the "central valley" (Fig. 1A). A second mound of light-
101 toned deposits is located between the central valley and the south-eastern rim of Ophir Chasma.
102 The geology of the LTDs was investigated by Nedell *et al.*, 1987 and Komatsu *et al.*, 1993, and a
103 geological map based on Viking imagery was provided by Lucchitta, 1999. According to these
104 authors, the chasmata of Valles Marineris probably formed as collapse structures along faults
105 that later widened to grabens into the surrounding Noachian to Hesperian aged plains, which are
106 built up by Tharsis-derived lava. By the time of the deposition of the LTDs, the chasm walls
107 were already eroded to the spur-and-gully morphology observable today, which indicates that the
108 deposition was clearly post-tectonic. Subsequently, the LTDs were heavily eroded by wind
109 and/or water action. The walls of the chasmata receded from the remaining LTD platforms, and
110 the resulting "moat" surrounding them was partly covered by landslides.

111 **2 Datasets and Methods**

112 **2.1 Hyperspectral data**

113 OMEGA and CRISM are both visible-short wave infrared imaging spectrometers. OMEGA
114 (Bibring *et al.*, 2004) is the mapping infrared spectrometer onboard ESA's Mars Express
115 spacecraft. It covers the wavelength range from 0.38 μm to 5.1 μm in 352 contiguous bands. The
116 data is acquired by three different channels, one for the visible to near infrared spectrum (0.38-
117 1.05 μm), a second for the spectral range from 0.93 to 2.73 μm and a third covering the range
118 from 2.55 to 5.1 μm . We used mostly data from 0.93 to 2.73 μm , as this range covers electronic
119 transition absorptions due to olivine and pyroxene (Adams, 1974, Cloutis and Gaffey, 1991,
120 Sherman *et al.*, 1982, Sunshine and Pieters, 1990), and vibrational absorptions in H₂O and/or
121 hydroxyl-bearing minerals such as phyllosilicates, hydrated sulfates and oxyhydroxides (Burns,

122 1993, Clark *et al.*, 1990). The spectral resolution of OMEGA is 20 nm in this wavelength range.
123 Due to Mars Express' highly elliptical orbit, the spatial resolution of OMEGA varies between
124 300 m and 3-4 km per ground element. Most of the OMEGA data used in this study have a
125 spatial resolution in the order of 600 to 700 m per ground element.
126 CRISM (Murchie *et al.*, 2007; 2009c) onboard NASA's Mars Reconnaissance Orbiter (MRO)
127 features a similar spectral range from 0.4 to 3.9 μm in 544 bands at a spectral resolution of 6.55
128 nm, recorded by two distinct detectors, the "S"-detector in the range of 0.39 to 1.02 μm , and the
129 "L" detector in the range of 1.02 to 3.92 μm wavelength. The data are acquired in several modes,
130 including the targeted mode at a spatial resolution of 18 m (FRT mode) or 36 m/pixel (HRL
131 mode) using all bands, or in multispectral mapping (MSP) mode at a spatial resolution of 200 m
132 per pixel using a subset of 72 selected spectral bands. We mostly used the data in the range of 1
133 to 2.6 μm , as this is the range where absorption bands of sulfates occur, but included the visible
134 range for the confirmation of the presence of ferric oxides. Table 1 provides the observation
135 numbers used here.

136

137 [INSERT TABLE 1 HERE]

138

139 The OMEGA and CRISM data were converted to I/F, divided by the cosine of the solar
140 incidence angle, and the CO_2 absorption features around 2 μm caused by the Martian atmosphere
141 were removed using the improved volcano-scan technique provided by McGuire *et al.*, 2009.
142 Noise in CRISM data was reduced using various filtering procedures (Parente, 2008). We used
143 the spectral indices or "summary products" (Bishop *et al.*, 2009; Murchie *et al.*, 2009b; Pelkey *et*
144 *al.*, 2007) on OMEGA and CRISM data to identify spectral features characteristic for specific

145 minerals or groups of minerals. Out of these, the index for a band at 1.9 μm due to combinations
146 of H_2O bending and stretching vibrations (BD1900), the 2.1 μm band depth (BD2100) the band
147 depth at 2.21-2.26 μm due to Si-OH vibrations (BD2210) and the index quantifying the spectral
148 convexity around 2.3 μm caused by H_2O absorptions (SINDEX) were particularly useful to
149 identify regions that required detailed spectral analysis.

150 Ferric oxide was identified by its strong increase in reflection between 1 and 1.3 μm , which we
151 calculated as the ratio between the reflectance at 1.2767 μm and the reflectance at 1.080 μm for
152 CRISM data and the ratio between reflectance at 1.2705 μm and 1.0837 μm for OMEGA data,
153 similar to Le Deit *et al.*, 2008; Mangold *et al.*, 2008. This index is sensitive to ferric oxides or
154 oxyhydroxides like hematite and goethite or mixtures containing these minerals, but also to iron
155 bearing sulfates, like, for example, copiapite. We therefore corroborated the presence of ferric
156 oxides using the spectral data in the visible-near infrared range from the CRISM S detector. To
157 this end, we excluded the spectral data shortward of 0.41 μm and longward of 0.97 μm as well as
158 the range between 0.64 and 0.69 μm due to known calibration problems in these regions of the
159 detector (Murchie *et al.*, 2009c). Spectra of Mars in the visible wavelength range are dominated
160 by the presence of nanophase ferric oxides. The detection of coarse-grained red hematite,
161 goethite or other ferric phase therefore requires the calculation of spectral ratios to a reference
162 spectrum in the same observation, which is spectrally unobscured and dominated only by
163 dust. These reference spectra were calculated as average spectra over a few hundreds or
164 thousands of pixels. The spectral bands of ferric oxides, ~ 0.53 and 0.86 μm for red hematite and
165 ~ 0.5 and 0.9 μm for other ferric phases, were then made visible by removing the continuum
166 separately in the range of 0.41 to 0.64 μm and 0.69 to 0.97 μm (Clark *et al.*, 1987). Further
167 evidence for the presence of ferric oxides in Ophir Chasma is the independent identification of

168 grey hematite in the thermal infrared by TES (Weitz *et al.*, 2008). Spectra in the range of 1 to 2.6
169 μm were averaged over regions of interest and either compared directly to laboratory spectra or
170 likewise ratioed to spectrally bland (dusty) regions. We used laboratory spectra of pure minerals
171 from the RELAB spectral library provided with the CRISM Analysis Tool (CAT).

172
173 An absorption band near 1.9 μm is found in various types of minerals: Hydrated silica, hydrated
174 sulfates, phyllosilicates and also carbonates show this spectral feature, which makes further
175 absorptions necessary to distinguish between these groups of minerals. Monohydrated sulfates
176 show an absorption near 2.1 μm , which is detected by the BD2100 index. The exact location of
177 this absorption band is at 2.13 μm for the magnesium-rich kieserite ($\text{MgSO}_4 \cdot \text{H}_2\text{O}$) and at 2.09
178 μm for the iron-rich szomolnokite ($\text{FeSO}_4 \cdot \text{H}_2\text{O}$). Both minerals also show an absorption at
179 2.4 μm (Cloutis *et al.*, 2006). A distinction between these two minerals was only attempted for
180 OMEGA and CRISM data at full spectral resolution. and not the multispectral data from CRISM,
181 as the generally higher noise level prevented an analysis to this detail.

182 Polyhydrated sulfates are identified by absorption bands at 1.45 and 1.95 μm and a drop-off in
183 reflectance near 2.4 μm . Absorptions in the 2.2-2.3- μm -region are indicative for hydrated silica,
184 phyllosilicates, or jarosite, and are attributed to OH-stretching and Si-OH bending. Hydrated
185 silica such as opal show a broad absorption band between 2.20 and 2.26 μm due to overlapping
186 bands caused by hydroxyl-groups and water molecules in the hydrate sphere. Jarosite is
187 identified by absorptions at 1.47, 1.85 and a doublet at 2.21 and 2.26 μm . Phyllosilicates show a
188 narrow absorption band in the wavelength region between 2.2 and 2.31 μm . Its exact position
189 allows a distinction between aluminum-rich clays like montmorillonite (2.20 μm), iron-rich
190 nontronite (2.28 μm), and magnesium-rich saponite (2.31 μm).

191 **2.2 Panchromatic and multispectral imagery**

192 The High Resolution Stereo Camera HRSC (Neukum and Jaumann, 2004) combines nine CCD
193 line detectors behind a common optics. The viewing directions of the detectors are oriented at
194 angles between -18.9 and $+18.9^\circ$ with respect to the nadir view, and four of the sensors are
195 equipped with broadband color filters for the red, green, blue and near infrared sections of the
196 spectrum. This design allows for the simultaneous acquisition of panchromatic images with a
197 map-projected ground resolution of up to 12.5 m per pixel, multispectral/color images and
198 panchromatic multiple stereo ground coverage to produce digital terrain models (DTM). The
199 resolutions of the color channels and the off-nadir panchromatic channels is usually reduced
200 onboard by a factor of two or four with respect to the nadir channel to reduce the amount of data
201 to be transferred to Earth (McCord *et al.*, 2007).

202 The HRSC color images have been beneficial for the mapping of the dark, basaltic sand dunes
203 and deposits (McCord *et al.*, 2007; Williams *et al.*, 2009), which have a bluish hue in color-
204 stretched RGB representations of the red, green and blue HRSC channels, and for the distinction
205 between Al- and Mg/Fe-rich clay minerals in Mawrth Vallis (Loizeau *et al.*, 2007). Although a
206 direct correlation between HRSC color spectra and specific minerals or rock types in other cases
207 is difficult, the subtle color variations in HRSC images can and should be used to distinguish
208 geologic units visually. We therefore used HRSC RGB representations of the red, green and blue
209 HRSC channel, pansharpened with the higher resolved panchromatic, nadir-viewing HRSC
210 channel or with CTX (Malin *et al.*, 2007) images in several occasions in this study.

211 We investigated the geometry of the LTDs based on digital elevation models (DTM) with spatial
212 resolutions of 50 or 100 m cell size, which were derived from individual HRSC orbits (Gwinner
213 *et al.*, 2000). We also used a regional DTM of the entire Valles Marineris at a resolution of 150 m
214 cell size, which was produced from several bundle-block-adjusted HRSC orbits (Dumke *et al.*,

215 2010). We estimated the attitude of observed layers by fitting a plane through three or more
216 points selected in the HRSC DTMs along the outcrop of the layering observed in the co-
217 registered imagery (similar to Zegers *et al.*, 2006) using the software tool developed by Kneissl
218 *et al.*, 2010. In addition to this, anaglyphs were produced directly from the HRSC nadir channel
219 and one of the stereo channels, as these products provide more topographical detail than a DTM
220 produced from the same data.

221 We also used panchromatic imagery from the Context Imager CTX (Malin *et al.*, 2007) with a
222 spatial resolution of approx. 6 m per pixel, and panchromatic and color images from the HiRISE
223 experiment (McEwen *et al.*, 2007) with a spatial resolution of up to 25 cm per pixel.

224 **3 Results**

225 **3.1 Overview**

226 Figure 1A shows Ophir Chasma as a false color mosaic of the red, green and blue channel of
227 HRSC. Figure 1B shows the mineral indices for iron oxides, sulfates (SINDEX) and
228 monohydrated sulfates (BD2100) calculated from OMEGA and CRISM data as a RGB image
229 overlain on a panchromatic HRSC mosaic. In this visualization, monohydrated sulfates appear in
230 a blue-green hue, polyhydrated sulfates have a green hue, and iron oxides are shown in red.
231 In the HRSC color image, dark, basaltic material appears with a bluish hue. It is found as a dune-
232 forming aeolian deposit in the central valley, the "mineral bowl", in wind traps along the
233 northern of Ophir Mensa and on top of the ILD east of the central valley. The basaltic sand
234 covers ILDs and landslides, its deposition therefore occurred after sulfate formation. The dark
235 material shows a spectral signature of pyroxenes and in the central valley of pyroxenes and
236 monohydrated (kieserite) deposits. Possible sources of the basaltic material are the eroding

237 chasm walls and landslide material, and a possible late-stage volcanism (Lucchitta, 2002). In
238 nearby western Candor Chasma, dark, basaltic material shows a spectral signature of
239 monohydrated sulfates, and HiRISE images show distinct, friable layers within the ILDs, from
240 which the basaltic sands are released by erosion (Murchie *et al.*, 2009a). Similar layers are not
241 found in Ophir Chasma. The ILDs appear to be mostly massive, without showing a layering
242 structure. Locally, dark bands are observed, e. g., east of the central valley. At close inspection,
243 these bands appear to be superficial, aeolian deposits on terraces caused by differential erosion
244 along layering in the ILDs, but not basalt-bearing layers *within* the ILDs. The fact that the
245 basaltic sand in the central valley shows spectral features of monohydrated sulfates does not
246 imply an origin of the basalts from within the ILDs, as suggested for western Candor Chasma, as
247 the sulfate signature is likely caused by the light toned kieserite deposits peeking through the
248 loose, dark sand cover. On the other hand, erosion of the chasm walls inevitably continued
249 during deposition of the ILDs independent of the depositional environment in the basin:
250 therefore, an incorporation of basaltic material into the ILDs most likely took place, but the lack
251 of distinct, dark layers suggests that this process played only a minor role. Consequently, the co-
252 occurrence of pyroxenes and sulfates does not imply a genetic relationship between the two
253 groups of minerals, which would allow a reconstruction of a common deposition.
254 Spectral signatures of iron oxides and sulfates are found only on a small fraction of the deposits
255 in Ophir Chasma, while most of the deposits are spectrally bland. Mangold *et al.*, 2008,
256 Chojnacki and Hynes, 2008, and LeDeit, 2008, observed, that sulfates are found only in
257 consolidated rocks with an elevated thermal inertia in TES data, and concluded that sulfates
258 might be much more pervasive within the LTDs, but undetectable due to a cover of
259 unconsolidated dust. This general trend is correct, but many locations are spectrally bland despite

260 relatively high thermal inertia values (Chojnacki *et al.*, 2006). This is the case for the ILD
261 material on the northern flank of Ophir Mensa, which shows an elevated thermal inertia, but is
262 nevertheless spectrally featureless in CRISM and OMEGA data. Although optically thick dust
263 deposits could mask spectral features in the visible and near infrared region and at the same time
264 hardly affect the thermal radiation, these locations are on steep flanks with deep erosional rills
265 and free of dunes in high-resolution imagery, which does not suggest a dust cover.

266
267 The locations of sulfate and ferric oxide detections can be divided into three groups based on
268 their stratigraphy with respect to Ophir Mensa. The observations in the west of Ophir Mensa
269 (Fig. 2) and on the northern side of the "mineral bowl" suggest the presence of sulfates within the
270 deposits of Ophir Mensa. On the southern wall of the "mineral bowl" (and Ophir Chasma), the
271 stratigraphic relationship to Ophir Mensa is not completely clear. The outcrops in the "moat"
272 north of Ophir Mensa and in the central valley form the third group of deposits, as they appear to
273 overlay, and thus postdate the formation and erosion of the bulk of the light-toned deposits
274 making up Ophir Mensa. All outcrops will be discussed in detail in the following text.

275 Figure 1A also shows the location of a prominent marker horizon within Ophir Mensa as a
276 dashed, red line. This horizon shows several curves and can be traced from the western end of
277 Ophir Mensa up to its base at the eastern end of the "mineral bowl" valley. It mostly forms a
278 steep cliff approx. 500 m high (Fig. 2). Layer attitude measurements along this horizon indicate
279 that the layering generally dips outward, following the topography of Ophir Mensa (compare to
280 Zegers *et al.*, 2006). In the west of Ophir Mensa, the horizon is located stratigraphically near the
281 top of the mound and dips approximately horizontally. In the center of Ophir Mensa, the horizon
282 appears to plunge at angles in the order of 5° underneath the stratigraphically higher deposits of

283 the eastern Ophir Mensa. Towards the flanks, dip angles increase to around 20°. A kink in the
284 slope is observed in the "mineral bowl", changing from 17° directly above the marker horizon to
285 values around 10° below it. Interestingly, the sulfate deposits within Ophir Mensa are only found
286 in the section beneath this horizon.

287

288 INSERT FIGURE 2 HERE

289

290 **3.2 Western Ophir Mensa**

291

292 Figure 3 shows a subset of the CRISM targeted observation FRT0000B27B in the western part
293 of Ophir Mensa. In this location, the LTDs show layering in the order of a few tens of meters in
294 thickness, which dip westward at moderate angles around 7°. Absorption bands near 1.6 μm ,
295 2.1 μm and at 2.4 μm suggest the presence of monohydrated sulfates such as kieserite. The
296 slightly lower albedo and the presence of small dunes in the region showing a presence of
297 polyhydrated sulfates (green) in the HiRISE image PSP_008458_1760 (Fig. 3B) suggests that
298 the boundary of kieserite detection, which does not coincide with the layering, is caused by the
299 thin dust coverage, and not by a change of the mineralogy of the rocks in these layers. This
300 suggests that the ILDs of Ophir Mensa above the marker horizon are sulfate-free, whereas the
301 detection below this horizon is controlled by the presence or absence of a masking dust cover.
302 Thus, in the lower part sulfates might be much more abundant, despite only limited detections in
303 orbital data.

304

305 **3.3 The "mineral bowl"**

306

307 [INSERT FIGURE 4 HERE]

308

309 The "mineral bowl" is the depression between Ophir Mensa and the southern wall of Ophir
310 Chasma. It extends approximately 70 km in East-West-direction and is up to 20 km wide (Fig.
311 4). It owns its informal name due to the complex relationship between spectrally bland ILDs of
312 Ophir Mensa and sulfates and crystalline ferric oxide detections within Ophir Mensa, on the
313 southern wall, and on the valley floor (Chojnacki and Hynek, 2008). The southern wall itself is
314 built up from layers of basaltic rocks (Lucchitta, 1999). The spatial and spectral resolution of the
315 CRISM and OMEGA data of this valley is very diverse. Therefore, the mineralogy of this
316 complex outcrop region can only locally be assessed in detail. We will provide an overview of
317 the mineral phases observed, before discussing the relationship between Ophir Mensa and the
318 southern chasm wall (Fig. 5) and between the southern chasm wall and the overlying LTDs (Fig.
319 6).

320 Starting in the eastern part of the northern slope of the valley, CRISM detects absorption bands
321 at 1.6, 2.13 and 2.4 μm consistent with kieserite at the base of Ophir Mensa and an erosional
322 remnant of Ophir Mensa approx. one km towards the center of the valley. These outcrops show
323 layering of tens of meters in thickness, and HiRISE imagery reveals even thinner internal
324 layering in the meters scale. The layers were interpreted as the source of crystalline ferric oxides
325 found in the dark material covering the floor of the valley (Weitz *et al.*, 2008). The sulfate and
326 hematite-bearing rocks form a bench, which is evidenced by a break in dip angles from approx.
327 17° in the sulfate-free ILDs above to 10° within the sulfate-bearing rocks. The floor of the
328 "mineral bowl" drops towards the south and is covered by dark material, which appears to be a

329 mixture of basaltic, pyroxene rich sand and crystalline ferric oxides, as evidenced by TES (Weitz
330 et al., 2008) and CRISM data. Several light-toned patches with a spectral signature of
331 monohydrated sulfates are found underneath this blanket. This suggests that the bench of sulfate-
332 rich material extends further south underneath the dark cover to the opposite slope of the valley.
333 In the center of the northern slope of the "mineral bowl", the sulfate-bearing bench forms a cliff
334 about 400 meters high. Polyhydrated sulfate deposits are observed near the top of the cliff,
335 monohydrated sulfate-rich deposits are found at the base and on the valley floor below. In the
336 western part of the "mineral bowl", the base of Ophir Mensa is heavily eroded and forms a deep
337 embayment towards the north, bound by steep flanks. OMEGA and CRISM data show kieserite
338 spectra on these walls up to an elevation of approximately +250 m. The observation of kieserite
339 spectra despite the heavy erosion suggests that fresh sulfates from within Ophir Mensa are
340 exposed, rather than being a thin surface coating on the Ophir Mensa slopes. On the valley floor,
341 layering of smooth, dark-toned, basaltic material and lighter-toned material with intermixed
342 sulfates and iron oxides can be observed. Locally, light-toned, sulfate-rich dunes are found.

343

344 [INSERT FIGURE 5 HERE]

345

346 The relationship between Ophir Mensa and the southern chasm wall is shown in Fig. 5.

347 Monohydrated sulfates are observed within the eroded base of Ophir Mensa and overlying the

348 spur-and-gully morphology of the southern chasm wall ("MHS in situ" in Fig. 5A), where they

349 are found from the foot of the slope at an elevation of ~-2200 m up to ~+800 m. The thickness of

350 the light-toned cover of the southern wall appears to increase from the top to the bottom of the

351 southern slope, suggesting downslope movement of material. Several light-toned ridges are

352 observed (white arrows in Fig. 5) covering the kieserite deposits, which have been described as
353 "pasted on" the underlying basaltic basement (Chojnacki and Hynek, 2008; Weitz *et al.*, 2008)
354 based on MOC imagery (Malin *et al.*, 1992). They are too small to be resolved in the CRISM
355 MSP data available here, but are very similar in texture to light-toned ridges further to the east,
356 (Fig. 6 and 7), showing a distinct mineralogy (see below). The kieserite on the southern slope of
357 the "mineral bowl" is overlain by rough-textured polyhydrated sulfates and locally ferric oxides.
358 The sulfate deposits on the southern wall end abruptly along an east-west-trending lineament we
359 interpret as a normal fault. Together with a parallel feature approx. two to three km northward it
360 forms a graben in the floor of the "mineral bowl" (center of Fig. 5A). The graben can be traced
361 further eastward as a depression with angular boundaries (top of Fig. 5B). The graben is filled
362 with smooth layers of monohydrated sulfates eroded from Ophir Mensa and the southern chasm
363 wall ("MHS, redeposited" in Fig. 5A). Partly, these monohydrated sulfate outcrops are covered
364 by spectrally bland material from further up the slope of Ophir Mensa.

365 The black arrows in Fig. 5 mark a "tongue shaped" deposit that bridges the gap between the
366 southern slope of Ophir Chasma and Ophir Mensa. It starts below the top of Ophir Mensa at
367 approx. 0 m elevation, stretches down the slope of Ophir Mensa to an elevation of ~-400 m, and
368 rises again to ~0 m on the southern wall of Ophir Chasma. This outcrop is covered only by
369 OMEGA data at a spatial resolution of 2.5 km/pixel and is partly overlain by smooth material,
370 but the textural similarity to outcrops further to the east suggests that it consists of kieserite and
371 is the westward prolongation of the kieserite deposits on the southern chasm wall ("MHS, in
372 situ" Fig. 5). If this is the case, this suggests that (1) at the time when light-toned deposits of
373 Ophir Mensa extended further to the south, as suggested by the monohydrated sulfates on the
374 southern wall and the southward continuation of the light-toned deposits underneath a basaltic

375 cover described in the eastern part of the "mineral bowl" (Fig. 5), these light-toned deposits
376 never filled up the "mineral bowl" to the top of Ophir Mensa, but instead, a valley existed at the
377 location of the "tongue-shaped" deposit between Ophir Mensa and the southern wall. It also
378 suggests, that (2) the polyhydrated sulfate deposits on the southern wall discordantly superpose
379 the kieserite deposits ("MHS in situ", Fig. 5) on the southern chasm wall. Further high resolution
380 HiRISE and CRISM observations of this part of the "mineral bowl" would help to solve this
381 case.

382 The diverse mineralogy and complex depositional pattern of the LTDs on the southern wall are
383 observed at the highest spectral and spatial resolution in the CRISM observation FRT0000A86A
384 in Fig. 6. It shows ridges of kieserite in the valley cut into the chasm wall (center of Fig. 6A).
385 These ridges, which could correspond to "MHS in situ" in Fig. 5, are overlain by a sequence of
386 smooth layers corresponding to "MHS, redeposited" in Fig. 5. The smooth layers dip downslope
387 at an angle of approx. 14° . Polyhydrated sulfates are found concordantly on the top of the
388 smooth layers, but at the foot of the slope, they discordantly superpose and embay a massive
389 outcrop of kieserite (Fig. 7A, C). Iron oxides are mostly associated with polyhydrated sulfates,
390 but they also occur directly on top of kieserite. We analyzed the ferric oxides further using the
391 CRISM data in the visible spectrum, as described in section 2. The regions appearing red in Fig.
392 5A show very similar spectral characteristics with a broad absorption band at $0.86 \mu\text{m}$ and two
393 minor bands at 0.5 and $0.58 \mu\text{m}$, resembling the spectrum of red hematite (Fig. 6G).

394

395

396 [INSERT FIGURE 6 HERE]

397

398

399

400 Three other mineral phases are detected in this CRISM observation as well. Phase one displays
401 spectral bands at 1.85 and 2.27 μm , diagnostic for jarosite, with the Fe-depleted H_3O -jarosite
402 (Milliken *et al.*, 2008) being the best match (blue in Fig. 6B). It is found in several locations
403 close to polyhydrated sulfates, both in the narrow valley and near the base of the slope. In the
404 visible spectral range, this material displays an asymmetric absorption band at 0.45 μm , which
405 fits to an absorption feature of jarosite at 0.44 μm . A second phase is characterized by
406 absorptions near 1.93 and 2.21 μm and a shoulder near 2.32 μm (2.21-phase). Its spectrum does
407 not match any of the laboratory spectra available from RELAB. Laboratory spectra with an
408 absorption near 2.2 μm include amorphous SiO_2 and Al-rich phyllosilicates like montmorillonite
409 (Fig. 5). However, amorphous SiO_2 shows a broad absorption band around 2.22 μm and no
410 shoulder towards longer wavelengths, while montmorillonite has a narrow absorption band at
411 2.21 μm and shoulder near 2.27 μm , which makes both minerals unlikely matches. Similar
412 spectra have been reported by Roach *et al.*, 2010b from Ius Chasma and elsewhere in Valles
413 Marineris, and have been interpreted as hydrated silica phases or mixtures of phyllosilicates,
414 amorphous silica and/or jarosite. A third phase has a very similar spectrum as the 2.21- μm -
415 phase, but shows an absorption band at 2.23 μm . This spectrum is similar to spectra observed in
416 Aram Chaos and interpreted as a ferric hydroxysulfate (Lichtenberg *et al.*, 2010), which was
417 produced in the laboratory by desiccation of synthetic melanterite ($\text{Fe}^{2+}\text{SO}_4 \cdot 7(\text{H}_2\text{O})$). Unlike any
418 other spectra in this observation, this material displays an absorption band at 0.76 μm (Fig. 5G).
419 The polyhydrated ferric sulfate coquimbite ($\text{Fe}^{3+}_2(\text{SO}_4)_3 \cdot 9(\text{H}_2\text{O})$, not shown) has a similar band
420 near 0.76 μm , but its spectrum does not match in the short wave infrared range. The 2.21- μm -

421 phase and the 2.23- μm -phase occur in similar stratigraphic positions. They superpose kieserite
422 deposits as a thin, very light-toned coating, and are covered by basaltic debris, as shown in Fig.
423 7 and the schematic cross-sections therein. The outcrop of the 2.23- μm -phase in Fig. 7A appears
424 to be more deeply eroded than the 2.21- μm -phase. It therefore is interpreted as underlying the 2.21-
425 μm -phase in the cross section in Fig. 7C. Polyhydrated sulfates are found in a similar
426 stratigraphic position overlying kieserite units. The basalts at the top of the ridge in Fig. 7B
427 appear blocky and layered, and thus resemble remnants of basaltic lava flows underlying the
428 sulfates rather than aeolian deposits on top of them. This ridge is very similar to ridges in the
429 west of the "mineral bowl" (white arrow in Fig. 5), suggesting that its mineralogy is present
430 elsewhere in this part of Ophir Chasma, but not detected due to the lack of high-resolution
431 spectral data.

432

433 [INSERT FIGURE 7 HERE]

434

435 **3.4 The "northern moat"**

436 The "northern moat" is the west-east-trending valley between Ophir Mensa and the northern rim
437 of Ophir Chasma. Its floor is mostly covered by landslides eroding the chasm wall. In a few
438 places, patches of light-toned material appear through windows in the landslide material cover
439 (Fig. 8). The two outcrops in Fig. 8 A and B have a texture similar to Ophir Mensa, which
440 suggests that Ophir Mensa once extended further northward. The two patches show no spectral
441 signature of sulfates, and are located at elevations of -3100 m and -3300 m, whereas a third patch
442 of light-toned material is found at -4600 m. This third patch is similar in texture to the floor of
443 the central valley. Ratioed CRISM MSP and OMEGA spectra show an absorption band at

444 1.4 μm , a broad feature at 1.9 μm and a drop-off in reflectance longward of 2.3 μm , consistent
445 with polyhydrated sulfate. The similar elevation, mineralogy and texture of this outcrop and the
446 deposits in the central valley suggests that unlike the two outcrops in Fig. 8A and B, this outcrop
447 is not a remnant of Ophir Mensa, but rather an infill of the basin between Ophir Mensa and the
448 northern chasm wall, similar to the central valley fill.

449

450 [INSERT FIGURE 8 HERE]

451

452 Sulfates are also found within the deposits of a landslide in Fig. 9. It shows sulfate-rich material
453 at the tip of a landslide fan that was deposited against the LTDs of Ophir Mensa. Since the time
454 of deposition of this landslide, the slope of Ophir Mensa has been eroded backward 1.2 to 2.5 km
455 by wind, leaving behind a flat, dune-covered plain between the landslide deposit and the slope of
456 Ophir Mensa. The HRSC anaglyph in Fig. 9B suggests that the landslide deposit and the sulfate
457 material therein overlay the light-toned deposits of Ophir Mensa, as shown in the cross-section in
458 Fig. 9C. Theoretically, the sulfates could have formed prior to the landslide event, or by water
459 released by the landslide event itself. Lucchitta, 1987, argued that the landslides in the central
460 valley of Ophir Chasma released large quantities of water, which caused the collapse of the
461 mountain barrier between Ophir and Candor Chasmata, and deepened the central valley.

462 However, Quantin *et al.*, 2004, observed, that landslides in Valles Marineris occurred at all times
463 between 3.5 Ga and 50 Ma before present, and that they always show the same characteristics.

464 This suggests that no water was involved in the formation of the landslides, as the atmospheric
465 conditions during this period did not allow a sustained existence of liquid water. The topographic
466 elevation of the sulfates of -3450 m is also much higher than the -4500 m of the closest sulfate

467 deposits in the "northern moat" (Fig. 8C). We therefore conclude that the sulfates in Fig. 9 were
468 formed prior to the landslide events. The ages of the landslides in Ophir Chasma range between
469 80 Ma and 1 Ga (Quantin *et al.*, 2004) and provide no constraint on ILD formation and water-
470 related activity, which ended at 3 to 3.5 Ga (Quantin *et al.*, 2010).

471

472 [INSERT FIGURE 9 HERE]

473

474 **3.5 The central valley**

475 The floor of the central valley is partly covered by sulfate-rich deposits, as shown in Fig. 10. Its
476 surface gently drops from -4250 m in the south-west to -4900 m in the north-east, resulting in a
477 dip of approximately 1° (Chojnacki and Hynek, 2008; Gendrin *et al.*, 2005; Mangold *et al.*,
478 2007). The deposits are at least 270 m thick, and are easily recognized by a distinct hue in HRSC
479 false color images (fig. 10D). The CRISM observations of this area generally confirm the
480 mineralogy derived from OMEGA data. The top of the deposit is dominated by the
481 monohydrated sulfate kieserite, that is partly covered by dunes of dark-toned, basaltic material. It
482 has a rough, fluted texture with curved ridges trending approximately perpendicular to the valley
483 axis (Fig 10E, F and G). An increase of the spectral slope between 1 and 1.3 μm in CRISM and
484 OMEGA spectra in the southern part of the valley indicates that the smooth material with an
485 intermediate albedo found in this part of the valley is rich in ferric oxides (fig. 10F).
486 Directly south of landslide deposits in the north of the central valley, the valley floor deposits
487 display spectra of polyhydrated sulfates. They show a fluted, wind-eroded topography (fig 10E),
488 but are devoid of the ridges found in the monohydrated sulfates (fig. 10F) and are not covered by
489 dark, basaltic dunes. The patch is topographically lower than the neighboring monohydrated-

490 sulfate rich deposits. This suggests that monohydrated sulfates overlay polyhydrated sulfates, as
491 shown in the cross-section in Fig. 10C. The superposition of monohydrated sulfates on top of
492 polyhydrated sulfates is contrary to sulfates in the "mineral bowl" and other chasmata of Valles
493 Marineris, such as Juventae Chasma (Bishop *et al.*, 2009; Gendrin *et al.*, 2005) and West Candor
494 Chasma (Murchie *et al.*, 2009a). The boundary between poly- and monohydrated sulfates is
495 gradational and coincides with a decrease in albedo from the brighter poly- to the slightly darker
496 monohydrated sulfates. However, it also coincides with an increase in the abundance of dark
497 dunes. Therefore, the albedo difference between the brighter polyhydrated sulfates and the darker
498 monohydrated (kieserite-dominated) sulfates (Chojnacki and Hynek, 2008), might be caused by
499 the presence of basaltic dunes and iron oxides in the area of the monohydrated sulfates, and not
500 by a color variation between the two sulfate species. Both sulfate species are not layered. The
501 deposit ends abruptly near the remains of the mountain barrier between Ophir and Candor
502 Chasma at 72° E, 5° S.

503

504 [INSERT FIGURE 10 HERE]

505

506 Light-toned, often subcircular patches with a diameter of a few hundred meters are observed in
507 the northern part of the central valley, where polyhydrated minerals are found (fig. 11). They
508 show bands at 1.93 μm , 2.21 μm and 2.27 μm and shoulder at 2.32 μm in CRISM targeted
509 observations, which is very similar to the 2.21- μm -phase observed in the "mineral bowl" (Fig. 6)
510 and Ius Chasma (Roach *et al.*, 2010b). Again, a mixture of jarosite (possibly H₃O-jarosite) and
511 amorphous silica or montmorillonite is the best spectral match. A phase with a band at 2.23 μm
512 is not observed here. Unlike the deposits in the "mineral bowl", the deposits in the central valley

513 are not layered, and almost indistinguishable from the surrounding deposits by their texture
514 alone.

515

516 [INSERT FIGURE 11 HERE]

517

518 **4 Discussion**

519 **4.1 Mineral detections**

520 Roach *et al.*, 2010b suggested four hypotheses for the minerals showing absorption bands at

521 2.21 μm observed in Ius Chasma, which are spectrally very similar to the 2.21- μm -phase

522 observed in Ophir Chasma: (1) a sulfate mineral structurally similar to jarosite, (2) amorphous

523 silica mixed with Fe-Mg-smectite, (3) a mixture of Al- and Fe-Mg-smectite, or (4) poorly

524 crystalline mixed Al-Fe clay formed either by acid alteration of clay minerals or as a direct

525 formation from dissolved basalt.

526 Library spectra of the three most common jarosite minerals, Na-jarosite, K-jarosite and H_3O -

527 jarosite, are very similar to the 2.21- μm -phase, but no perfect spectral match. Like the unknown

528 phase, they display absorptions at 1.93 μm and a shoulder near 2.32 μm , but the band at 1.85 μm ,

529 characteristic for jarosites, is not observed in the unknown phase. An absorption band at 2.21 μm

530 is observed in K-jarosite, but this mineral shows a second, deeper absorption near 2.27 μm ,

531 which is absent or only weakly expressed in the unknown phases. Therefore, if a jarosite mineral

532 is present in these phases, it is probably mixed with a different mineral.

533 Amorphous silica displays a broad spectral band at 2.21 μm , and a shoulder at 2.26 μm . In

534 contrast, the absorption band at 2.21 μm of the unknown phase is narrow, and its right shoulder

535 is located at longer wavelengths at 2.32 μm , which makes pure amorphous silica a bad spectral
536 match. A mixture of Al-rich and Mg/Fe-rich clay minerals or of clay minerals and jarosite could
537 reproduce the absorption bands observed here. However, clays form under circum-neutral pH-
538 conditions, whereas the clear identification of jarosite in neighboring locations, and partly in
539 similar stratigraphic positions, points towards acidic conditions (pH < 3-4, Papike *et al.*, 2006),
540 which makes the presence of clay minerals unlikely. A theoretical alternative would be the
541 formation of clay minerals at a different location than the jarosite minerals and subsequent
542 transport to this place, but the location of the 2.21- μm -phase high on the slopes just below the
543 crests of fresh basaltic wall rock effectively rules out this option, as it suggests a formation of
544 this phase *in situ*.

545 The last hypothesis is the formation as a poorly crystalline Fe-SiO₂-phase by acidic to neutral
546 leaching of nontronite, which would produce Si-OH vibrations due to the formation of
547 amorphous silica as in clay-rich material exposed to acidic vapors at Mauna Kea (Swayze,
548 unpublished data in Roach *et al.*, 2010b). This mechanism would also explain the observed
549 2.23 μm band observed locally during this study due to FeAlOH vibrations. Alternatively, Tosca
550 *et al.*, 2008, report the formation of a poorly crystalline Fe-SiO₂-phase as a precipitate from
551 dissolved basalt by addition of S and Cl under oxidizing conditions at a pH of 5-7 in laboratory
552 tests, which would possibly display similar spectral bands between 2.21 and 2.26 μm .

553 Of the proposed mineralogies of the unknown 2.21- μm -phase, we favor a mixture of jarosite and
554 amorphous silica or jarosite and a newly formed, poorly crystalline Fe-SiO₂- phase, and a
555 mixture of jarosite and a poorly crystalline Fe-Al-SiO₂-phase for the locations showing a
556 2.23 μm absorption, rather than mixtures of different phyllosilicate minerals or phyllosilicate
557 minerals and jarosite. In the "mineral bowl" (fig. 6), the clear identification of H₃O-jarosite

558 suggests acidic conditions, which are inconsistent with clay formation. Amorphous silica in
559 combination with jarosite has also been identified by CRISM on the plateau above Juventae
560 Chasma (Bishop *et al.*, 2009; Milliken *et al.*, 2008) and in Melas Chasma (Metz *et al.*, 2009),
561 where they are interpreted as the product of acidic alteration of basalts.

562 On Earth, jarosite and amorphous silica are known from acid mine drainage deposits, for
563 example in Spain (i.e., Sánchez España *et al.*, 2005) and Greece (Triantafyllidis and Skarpelis,
564 2006), where the oxidation of sulfides produces sulfuric acid, which in turn dissolves olivines,
565 pyroxenes and feldspars in the basaltic rocks to form jarosite, leaving behind amorphous silica
566 and kaolinite as the least soluble minerals. A similar mechanism has been proposed for Mars
567 (Burns, 1987; Burns and Fisher, 1990; Poulet *et al.*, 2008). Investigations on a Martian meteorite
568 show that a part of the jarosite and amorphous silica on Mars formed under hydrothermal
569 conditions (McCubbin *et al.*, 2009), but the H₃O-jarosite best matching the spectra from Ophir,
570 Melas and Juventae Chasma indicates temperatures below 100°C (Milliken *et al.*, 2008). All
571 jarosite species indicate a limited water supply and short time for the chemical alteration, as the
572 acidity is not neutralized by the decomposition of feldspars (Höller, 1967; Madden *et al.*, 2004).

573 H₃O-jarosite forms at even lower water/rock ratios, when sulfide minerals dissolve more rapidly
574 than rock forming minerals, resulting in a lack of Na and K with respect to Fe in the solution,
575 which prevents the formation of K- and Na-jarosite (Brophy and Sheridan, 1965). At rising pH,
576 H₃O-jarosite becomes unstable, and goethite (FeOOH) forms, while the sulfate ions go back into
577 solution (Burns and Fisher, 1990). At the same time, poorly crystalline Fe- or FeAl-SiO₂-phases
578 can form (Tosca *et al.*, 2008), which can be considered precursors to clay minerals. Goethite can
579 later transform into hematite, while the sulfate ions could precipitate as polyhydrated sulfates
580 upon evaporation of the brine. An alternative source for the acidity required for the jarosite

581 formation other than weathering of sulfides are volcanic, SO₂-rich exhalations as observed at the
582 Kilauea volcano (Schiffman *et al.*, 2006).

583 The mineral assemblage observed on the southern wall of Ophir Chasma (fig. 6 and 7) is
584 consistent with an acidic alteration of basaltic rock: jarosite and the unidentified, possibly
585 jarosite-amorphous silica bearing phases are almost always observed at the top of the hillsides,
586 just below the crest, locations that would have received very little water. They are covered by
587 basaltic debris, which would be the source rock. They are topographically higher than iron oxide
588 detections and polyhydrated sulfates, which would represent the more developed alteration
589 products. On the northern side of the mineral bowl, where the slopes are lacking a basaltic cover,
590 no 2.21- μ m-phase or jarosite are found. In the central valley, the relationship between the
591 abundant polyhydrated sulfates and the patchy outcrops of the 2.21- μ m-phase is not clear and
592 gives no hint on the formation history. A possible source rock for the sulfatic alteration products
593 cannot be identified.

594 **4.2 Stratigraphic relationships**

595 Any hypothesis for the formation of the light-toned deposits and the role of water therein has to
596 meet the constraints imposed by the stratigraphic relationships within the LTD units and between
597 the LTDs and the wall rocks. They are visualized in Fig. 12 and summarized as follows:

598 (1) All light-toned deposits in Ophir Chasma superpose the spur-and-gully morphology of the
599 canyon walls. Their deposition therefore postdates the formation of the chasm (Chojnacki and
600 Hynek, 2008).

601 (2) The LTDs of Ophir Mensa can be divided into two units based on layer boundaries and
602 mineralogy. A marker horizon (fig. 1) separates the two units. Its dip roughly follows the local
603 topography, with steep ($\sim 20^\circ$) slopes at the flanks of Ophir Mensa and approx. horizontal

604 layering in the center. This implies that the eastern part of Ophir Mensa is younger than the
605 western part.

606 (3) The lower unit of Ophir Mensa is kieserite-bearing. The strong erosion of Ophir Mensa in the
607 "mineral bowl" suggests that the kieserite signature is not a superficial deposit draped over a
608 sulfate-free rock, but that the entire lower unit contains kieserite sulfate.

609 (4) The monohydrated sulfates on the southern wall of the "mineral bowl" are connected to Ophir
610 Mensa by a "tongue" of light-toned, sulfate-rich material. This suggests that these deposits are of
611 the same age. The monohydrated sulfates in the "mineral bowl" therefore formed, when Ophir
612 Mensa extended further southward up to the southern wall of the chasm. The top of the LTDs
613 along the southern wall of Ophir Chasma dropped from west to east, as shown by remnants of
614 light-toned material on the chasm wall.

615 (5) However, at the time of sulfate formation, a precursor valley of the "mineral bowl" already
616 existed, which formed a depression between the center of Ophir Mensa and the southern wall.
617 This is shown by the (likely) sulfate-bearing "tongue" between the southern wall and Ophir
618 Mensa: It starts near the top of Ophir Mensa, drops down at its center and raises again towards
619 the southern wall (fig. 5B).

620 (6) Polyhydrated sulfates in the "mineral bowl" are found near the top of the light-toned material.
621 The transition between kieserite and polyhydrated sulfates appears concordant on the upper slope
622 of the southern wall (fig. 6 and 7), but discordant in the lower parts, where polyhydrated sulfates
623 embay an eroded remnant of kieserite-rich rock. Further westward, the polyhydrated sulfates
624 appear to discordantly overlay parts of the "tongue" between Ophir Mensa and the southern wall.
625 This implies that polyhydrated sulfates formed after the deposition and partial erosion of the
626 kieserite-rich rocks.

627 (7) It is not clear if the polyhydrated sulfates precipitated directly in their current form, or if they
628 formed by hydration of the underlying kieserite-rich material. The presence of jarosite and
629 poorly constrained, probably amorphous silica-rich material underneath a cover of basaltic debris
630 is consistent with an acid alteration of the basaltic cover caused by the decomposition of sulfides,
631 as suggested by Burns, 1987. This would require the presence of water, which could also have
632 transformed monohydrated kieserite to polyhydrated sulfates. An alteration from kieserite to
633 polyhydrated sulfates has also been suggested for Ius Chasma (Roach *et al.*, 2010b), whereas the
634 variation in sulfate mineralogy in Candor and Juventae Chasma has been interpreted to be caused
635 by changes of the composition of the evaporating brine (Murchie *et al.*, 2009a, Bishop *et al.*,
636 2009).

637 (8) Ferric oxides contained within the sulfate-rich deposits in Ophir Mensa (Bibring *et al.*, 2007)
638 accumulate on the floor of the "mineral bowl", where they form a partly indurated lag deposit
639 together with sulfates and basaltic debris from the south wall.

640 (9) The sulfates of the central valley and the "northern moat" show distinct characteristics. They
641 formed after the incision of the central valley, and therefore post-date Ophir Mensa.

642 (10) All sulfate deposits in the central valley are found below -4250 m, approx. 1450 m below
643 the lowest sulfate detections in the "mineral bowl". Only the sulfates underneath a landslide in
644 the "northern moat" are found at higher elevations (fig. 8), but it is not clear if they formed *in situ*
645 or have been transported to this elevation by the landslide.

646 (11) In the central valley, monohydrated kieserite apparently stratigraphically superposes
647 polyhydrated sulfates, unlike in Candor Chasma, Aram Chaos and Juventae Chasma, where
648 monohydrated sulfates are stratigraphically below polyhydrated sulfates (Bishop *et al.*, 2009;
649 Lichtenberg *et al.*, 2010; Murchie *et al.*, 2009a), but similar to Ius Chasma (Roach *et al.*, 2010b).

650

651 [INSERT FIGURE 12 HERE]

652

653 **4.3 Implications for formation hypotheses**

654 The presence of sulfates within the ILDs of Ophir Mensa indicate, that water played a role in
655 their formation. On the other hand, large parts of the ILDs are spectrally bland although they are
656 likely not covered by dust, as indicated by elevated TI values around 500 thermal inertia units
657 (Chojnacki and Hynek, 2008, fig. 2a), steep slopes and no visible small dunes in HiRISE images.
658 Therefore, these parts of the LTDs must either have formed under dry conditions that did not
659 involve water, or they are cemented by minerals that are not detectable from orbit, such as halite
660 (NaCl) or anhydrite (CaSO₄). In the following paragraphs, we will discuss the formation of the
661 ILDs in the light of our observations, before we investigate, whether the sulfates in Ophir
662 Chasma precipitated from evaporating groundwater (Roach *et al.*, 2010b; Rossi *et al.*, 2008) or
663 lakes (Lucchitta, 2009a; 2009b; McKay and Nedell, 1988) or meteoric water, or a combination
664 of these processes.

665 Some authors suggested that the LTDs were exhumed light-toned material from the chasm walls
666 (Adams *et al.*, 2009; Malin and Edgett, 2000). This idea can be rejected, as the light-toned
667 material clearly overlays the spur-and-gully morphology of the chasm walls as elsewhere in
668 Valles Marinieris (Blasius *et al.*, 1977; Lucchitta *et al.*, 1992; Nedell *et al.*, 1987). The idea that
669 the LTDs are subice volcanoes was proposed by Chapman and Tanaka, 2001. This theory
670 explains the outward dipping layers of the LTDs and the fact that most LTDs form free-standing
671 mounds, separated from the chasm walls by depressions. However, it implies that the LTDs are

672 volcanic strata. This is contradictory to the lack of a basaltic spectral signature of these rocks and
673 the missing of clear volcanic morphologies such as craters or lava flows.

674 If the LTDs were eolian or pyroclastic deposits (Chapman and Tanaka, 2001; Peterson, 1981),
675 we would expect similar deposits outside Valles Marineris (Glotch and Rogers, 2007). Layered
676 deposits deposits are found on the plains surrounding Valles Marineris (Bishop *et al.*, 2009,
677 Milliken *et al.*, 2008, Le Deit *et al.*, 2010), which are interpreted as airfall deposits (Le Deit *et*
678 *al.*, 2010). These deposits are much thinner (<100 m) than the deposits within the chasmata.

679 Thus, an origin of the spectrally bland material in the LTDs by airfall, either as volcanic clasts or
680 windblown dust, is conceivable, but an additional mechanism to trap and lithify these deposits is
681 required to explain the observed thickness of the deposits (Lucchitta, 2009a, 2009b).

682 Regardless of the origin of the spectrally bland LTDs, the sulfates within them are formed by
683 water. The stratigraphic relationships described in section 4.2 require at least two phases of
684 sulfate formation. In a first phase, sulfates formed within Ophir Mensa and in a second phase the
685 in the central valley. The monohydrated sulfates on the southern wall of Ophir Chasma appear to
686 be remnants of the sulfates of Ophir Mensa, which once extended further southward. The
687 polyhydrated sulfates possibly formed later, either by alteration of the previous monohydrated
688 sulfate, or by acid weathering of the overlying basaltic debris. The timing of this alteration
689 phase is poorly constrained. It can be contemporaneous with the sulfate formation in the central
690 valley and the northern moat, or might also have taken place independently from that event. For
691 nearby Capri Chasma, Roach *et al.*, 2010a advocated the concept that the monohydrated kieserite
692 was not the sulfate phase that initially precipitated, but was formed later during diagenesis from
693 previously polyhydrated sulfates under the overburden of several kilometers of sediments on top.

694 The LTDs of Ophir Mensa are several kilometers thick, therefore, diagenetic processes or

695 intrusions of brines that altered an initial mineralogy to the mineralogy now observed is possible,
696 but an assessment of their role is difficult and remains an open question.

697 The idea that the sulfates formed in lakes (Lucchitta, 2009a; 2009b; Peterson, 1981) implies that
698 the lakes acted as a trap for clastic deposits. The sulfates therefore would have formed at the
699 same time as the spectrally bland clasts hosting them. If this was the case, we would expect
700 horizontal layering and a constant upper elevation of the sulfate detection, which would resemble
701 the water level in the lake. The upper part of the LTDs, which is sulfate-free, would have been
702 formed by a different process. Therefore, the elevation variations of the upper sulfate detection
703 limit in the "mineral bowl" and the lack of sulfate detections in the LTDs at similar elevations on
704 the northern and eastern flank of Ophir Mensa are better explained by a formation by
705 groundwater (Murchie *et al.*, 2009a) that entered the LTD mound after its deposition. In this
706 case, the variations in elevation of the sulfate detections and the coexistence of sulfate-bearing
707 and sulfate-free LTDs at the same elevation would reflect the initial morphology of the hosting
708 sediments in the chasm, or variations of their permeability.

709 The deposits in the central valley are almost horizontal, which is consistent with a formation in a
710 lake as well as a playa, similar to the mechanism proposed for Meridiani Planum (Arvidson *et*
711 *al.*, 2003). The slight dip towards the north would either imply a dip of the sediments after
712 deposition, possibly by downfaulting of the entire chasm floor along the northern rim, or simply
713 deposition on an inclined chasm floor. The remnants of the collapsed mountain ridge between
714 Ophir and Candor Chasma could have acted as a barrier to form a lake behind it. The low
715 elevation of the sulfate deposit, implied by sulfate detections restricted to elevations below -4250
716 m, is consistent with the proposed lake in central Valles Marineris/Coprates Chasma with a
717 maximum ponding level at -3560 m proposed by Harrison and Chapman, 2008. The flanks of the

718 central valley show rills on both sides. Similar structures in Candor have been interpreted by
719 Murchie *et al.*, 2009a, as braided channels formed by flowing water. If this was the case in Ophir
720 Chasma, they could have acted as pathways for water entering the suggested lake. The rills have
721 also been interpreted to be formed by glacial scouring (Chapman and Smellie, 2007; Roach,
722 2009), which would also be consistent with a (frozen) lake in the central valley. However, the
723 rills may also have formed by wind erosion: Many of them are not perfectly perpendicular to the
724 slope of the hillsides they form in, but curve southward. This is a strong indication for wind
725 erosion rather than flowing water or ice.

726 Like in the central valley, polyhydrated sulfates are found topographically below monohydrated
727 sulfates in western Candor Chasma and Aram Chaos (Lichtenberg *et al.*, 2010; Murchie *et al.*,
728 2009a). In these locations, the polyhydrated sulfates have been interpreted as late-stage
729 sediments that were deposited discordantly in low-lying areas after erosion of the monohydrated
730 sulfates, so they would be stratigraphically above the monohydrated sulfate-rich deposits. In the
731 central valley, we do not see evidence for this interpretation. The boundary between mono- and
732 polyhydrated sulfates is transitional, and no unconformity is observed. We therefore interpret
733 that the topographically low polyhydrated sulfates are also stratigraphically below the
734 monohydrated sulfates. This stratigraphy has also been inferred for mono- and polyhydrated
735 sulfates in Ius Chasma (Roach *et al.*, 2010b).

736 The sulfates on the southern wall of the "mineral bowl" are spread over a wide range of
737 elevations, and dip downslope. This, and the "tongue" between Ophir Mensa and the southern
738 wall, implies that the "mineral bowl" depression existed already at the time of the deposition of
739 these sulfates. Even if Ophir Mensa once extended further southward, it would already have been
740 eroded away at least partly, as otherwise the layering of the deposits on the southern wall would

741 be more horizontal. If the sulfates were formed in a lake, this lake would have to have been deep
742 enough to form sulfates very high on the slope. In this case, other parts of this valley would have
743 been submerged at the same time, and should therefore show sulfate deposits too, which have not
744 been observed. The formation by evaporating groundwater would require that a groundwater
745 discharge from the entire slope of the chasm wall: water leaking from the top of the wall would
746 not have reached the debris deposits below the basaltic rocks on the "spurs" of the wall, where
747 some of the sulfates are found (fig. 7). The presence of high water tables in the narrow mountain
748 ridge between Ophir and Candor Chasma is also not likely. Therefore, if these deposits are
749 indeed acid alteration products of basalt, which is consistent with the spectral observations of
750 jarosite, amorphous silica, ferric oxides, polyhydrated sulfates and possibly poorly crystalline Fe-
751 SiO₂- or Fe-Al-SiO₂-phases (the 2.21- μ m-phase and the 2.23- μ m-phase), the best way to explain
752 the supply of water to the locations where these minerals are found, would be rain, snow or frost.
753
754 Glaciers in Valles Marineris, which could provide the required water, and could also explain the
755 variable range of elevations where water has been present, have been proposed in previous
756 studies (Chapman and Smellie, 2007; Chapman and Tanaka, 2001; Chapman and Tanaka, 2002;
757 Mège and Bourgeois, 2010), but in this particular location, associated landforms such as U-
758 shaped valleys are missing. A second source for water could be the fog clouds in Valles
759 Marineris (i.e., Moehlmann *et al.*, 2009). If the Martian soil contains perchlorates, as suggested
760 by results from the Phoenix lander (Zorzano *et al.*, 2009), these hygroscopic minerals would
761 attract water from the fog clouds in Valles Marineris and allow liquid water at temperatures as
762 low as 225°K. However, if this is indeed the process responsible for the alteration, it remains

763 unclear why it would be constrained to this part of Ophir Chasma only, as other parts of the
764 LTDs in the same chasm at similar elevations did not develop a spectral hydration signature.

765 **5 Conclusions**

766 Our study confirms and refines, based on OMEGA and CRISM data, previous studies based on
767 OMEGA data alone (Chojnacki and Hynek, 2008; Gendrin *et al.*, 2005; Mangold *et al.*, 2007).
768 Water-related minerals in Ophir Chasma are found mainly in two locations: In the "mineral
769 bowl" valley between Ophir Mensa and the southern wall, and on the central valley floor. The
770 same minerals are observed in these two locations, kieserite, polyhydrated sulfates, iron oxides
771 and newly discovered phases that are consistent with mixtures of jarosite and amorphous silica or
772 other poorly crystalline phases, but the two deposits are very distinct (Chojnacki and Hynek,
773 2008). In the "mineral bowl", kieserite is found in the bulk material of Ophir Mensa and on the
774 southern wall, where it could represent remnants of Ophir Mensa, which once extended further
775 southward. The variations in elevation of these sulfates are best explained by a post-depositional
776 alteration of clastic material of unknown origin, possibly airfall deposits, by ground water rather
777 than an open water body. On the southern wall, kieserite is superposed by H₃O-jarosite, and/or
778 possible jarosite-amorphous-silica mixtures with spectral bands at 2.21 μm or 2.23 μm,
779 polyhydrated sulfates and iron oxides. This sulfate deposit is layered, dips downslope, is
780 stretched over a wide range of elevations, and could be stratigraphically discordant to the
781 underlying bulk LTDs. Its formation therefore possibly took place after the excavation of the
782 "mineral bowl" valley. A similar succession of polyhydrated sulfates discordantly on top of
783 monohydrated sulfates in local depositional traps has been observed in western Candor Chasma
784 and Aram Chaos (Lichtenberg *et al.*, 2010; Murchie *et al.*, 2009a). In Candor Chasma, rills that

785 show similarities to braided river beds on the slopes of LTD mounds have been interpreted as
786 evidence of springs relatively high up the slopes of the chasm, which would have supplied the
787 water that eventually deposited the polyhydrated sulfates. In Ophir Chasma, locations of the
788 polyhydrated sulfates and the phases with absorptions at 2.21 or 2.23 μm on ridges of the
789 underlying basaltic material is neither consistent with a water supply scenario nor with an open
790 lake: therefore, meteoric water in the form of snow, frost or fog might have played a role. Debris
791 from the LTDs, including iron oxides, are found as lag deposits on the floor of the valley, where
792 they mix with basaltic material (Bibring *et al.*, 2007; Chojnacki and Hynek, 2008; Weitz *et al.*,
793 2008). On the northern side, the lack of CRISM targeted observations prevents a detailed spectral
794 analysis.

795 The sulfates in the central valley form a flat deposit at low elevations (< -4250 m), but appear to
796 be stratigraphically higher than Ophir Mensa's LTDs. These deposits are not layered, show
797 ridges or joints, and kieserite superposes polyhydrated sulfates. The polyhydrated sulfates
798 contain outcrops a few hundred meters in diameter of an unidentified mineral phase spectrally
799 consistent with a jarosite-amorphous-silica mixture. A deposition of these deposits in a lake,
800 possibly behind a mountain barrier that once separated Candor and Ophir Chasma, or in a playa-
801 like environment as in Meridiani Planum is conceivable.

802 The proposed succession of events is very similar to the suggested history of western Candor
803 Chasma, where the bulk of the sulfates in the LTDs is formed by intruding groundwater, and a
804 lesser amount of sulfates is formed by fluvial processes after excavation of the valleys cross-
805 cutting the ILDs by outflow events (Murchie *et al.*, 2009a, Fig. 9). However, in Ophir Chasma,
806 the excavation of the central valley is not necessarily an outflow event, but possibly caused by
807 glaciers. We do not observe convincing evidence for fluvial activity.

808

809 **Acknowledgements**

810 The authors like to thank Leah Roach and an anonymous reviewer for their comments, which
811 greatly helped to improve the manuscript. The study has been funded in part by the German
812 Space Agency (DLR Bonn) grant 50QM301 (HRSC on Mars Express) financed by the German
813 Federal Ministry of Economics and Technology and the Helmholtz Alliance “Planetary
814 Evolution and Life”. L. W. and C. G. thank Giuseppe Marzo for fruitful discussions on the
815 spectral data. P. C. M. would like to acknowledge support from the Alexander-von-Humboldt
816 Foundation and from the CRISM Science Team.

817

818 **References**

- 819 Adams, J. B., 1974. Visible and near-infrared diffuse reflectance spectra of pyroxenes as applied
820 to remote sensing of solid objects in the solar system. *J. Geophys. Res.* 79, 4829-4836.
- 821 Adams, J. B., Gillespie, A. R., Jackson, M. P. A., Montgomery, D. R., Dooley, T. P., Combe, J.
822 P., Schreiber, B. C., 2009. Salt tectonics and collapse of Hebes Chasma, Valles
823 Marineris, Mars. *Geology* 37, 8, 691-694.
- 824 Arvidson, R. E., Seelos, F. P., Deal, K. S., Koeppen, W. C., Snider, N. O., Kieniewicz, J. M.,
825 Hynek, B. M., Mellon, M. T., Garvin, J. B., 2003. Mantled and exhumed terrains in Terra
826 Meridiani, Mars. *J. Geophys. Res. (Planets)* 108, E12, 8073.
- 827 Bibring, J. P., Arvidson, R. E., Gendrin, A., Gondet, B., Langevin, Y., Le Mouelic, S., Mangold,
828 N., Morris, R. V., Mustard, J. F., Poulet, F., Quantin, C., Sotin, C., 2007. Coupled Ferric
829 Oxides and Sulfates on the Martian Surface. *Science* 317, 1206-1210.
- 830 Bibring, J. P., Soufflot, A., Berthé, M., Langevin, Y., Gondet, B., Drossart, P., Bouyé, M.,
831 Combes, M., Puget, P., Semery, A., Bellucci, G., Formisano, V., Moroz, V., Kottsov, V.,
832 Bonello, G., Erard, S., Forni, O., Gendrin, A., Manaud, N., Poulet, F., Poulleau, G.,
833 Encrenaz, T., Fouchet, T., Melchiori, R., Altieri, F., Ignatiev, N., Titov, D., Zasova, L.,
834 Coradini, A., Capaccioni, F., Cerroni, P., Fonti, S., Mangold, N., Pinet, P., Schmitt, B.,
835 Sotin, C., Hauber, E., Hoffmann, H., Jaumann, R., Keller, U., Arvidson, R., Mustard, J.,
836 Forget, F., 2004, OMEGA: Observatoire pour la Minéralogie, l'Eau, les Glaces et
837 l'Activité. *Mars Express: the Scientific Payload*, 37-49.
- 838 Bishop, J. L., Parente, M., Weitz, C. M., Noe Dobrea, E. Z., Roach, L. H., Murchie, S. L.,
839 McGuire, P. C., McKeown, N. K., Rossi, C. M., Brown, A. J., Calvin, W. M., Milliken,
840 R., Mustard, J. F., 2009. Mineralogy of Juventae Chasma: Sulfates in the light-toned
841 mounds, mafic minerals in the bedrock, and hydrated silica and hydroxylated ferric
842 sulfate on the plateau. *J. Geophys. Res. (Planets)* 114.

- 843 Blasius, K. R., Cutts, J. A., Guest, J. E., Masursky, H., 1977. Geology of the Valles Marineris -
844 First analysis of imaging from the Viking 1 orbiter primary mission. *J. Geophys. Res.* 82,
845 4067-4091.
- 846 Brophy, G. P., Sheridan, M. F., 1965. Sheridan, Sulfate studies IV: The jarosite-natrojarosite-
847 hydronium jarosite solid solution series. *Am. Mineral.* 50, 1595-1607.
- 848 Burns, R. G., 1987. Ferric sulfates on Mars. *J. Geophys. Res.* 92, E570-E574.
- 849 Burns, R. G., 1993. Origin of electronic spectra of minerals in the visible to near-infrared region.
850 in: C. M. Pieters, P. A. J. Englert, (Eds.), *Remote Geochemical Analysis: Elemental and*
851 *Mineralogical Composition*. Cambridge University Press, New York, pp. 3-29.
- 852 Burns, R. G., Fisher, D. S., 1990. Iron-sulfur mineralogy of Mars - Magmatic evolution and
853 chemical weathering products. *J. Geophys. Res.* 95, 14415-14421.
- 854 Chapman, M. G., Smellie, J. L., 2007. Mars Interior layered deposits and terrestrial sub-ice
855 volcanoes compared: observations and interpretations of similar geomorphic
856 characteristics. in: M. G. Chapman, (Ed.), *The Geology of Mars*. Cambridge University
857 Press, Cambridge, pp. 178-210.
- 858 Chapman, M. G., Tanaka, K. L., 2001. Interior trough deposits on Mars: Subice volcanoes? *J.*
859 *Geophys. Res.* 106, E5, 10087-10100.
- 860 Chapman, M. G., Tanaka, K. L., 2002. Related Magma-Ice Interactions: Possible Origins of
861 Chasmata, Chaos, and Surface Materials in Xanthe, Margaritifer, and Meridiani Terrae,
862 Mars. *Icarus* 155, 324-339.
- 863 Chojnacki, M., Hynek, B. M., 2008. Geological context of water-altered minerals in Valles
864 Marineris, Mars. *J. Geophys. Res. (Planets)* 113, E12, 12005.
- 865 Chojnacki, M., Jakosky, B. M., Hynek, B. M., 2006. Surficial properties of landslides and
866 surrounding units in Ophir Chasma, Mars. *J. Geophys. Res. (Planets)* 111, E4, 04005.
- 867 Christensen, P. R., Anderson, D. L., Chase, S. C., Clark, R. N., Kieffer, H. H., Malin, M. C.,
868 Pearl, J. C., Carpenter, J., Bandiera, N., Brown, F. G., 1992. Thermal emission
869 spectrometer experiment - Mars Observer mission. *J. Geophys. Res.* 97, E5, 7719-7734.
- 870 Clark, R. N., King, T. V. V., Gorelick, N. S., 1987, Automatic continuum analysis of reflectance
871 spectra. Third Airborne Imaging Spectrometer Data Analysis Workshop. JPL Publication,
872 138-142.
- 873 Clark, R. N., King, T. V. V., Klejwa, M., Swayze, G. A., Vergo, N., 1990. High spectral
874 resolution reflectance spectroscopy of minerals. *J. Geophys. Res.* 95, 12653-12680.
- 875 Cloutis, E. A., Gaffey, M. J., 1991. Pyroxene spectroscopy revisited - Spectral-compositional
876 correlations and relationship to geothermometry. *J. Geophys. Res.* 96, 22809-22826.
- 877 Cloutis, E. A., Hawthorne, F. C., Mertzman, S. A., Krenn, K., Craig, M. A., Marcino, D.,
878 Methot, M., Strong, J., Mustard, J. F., Blaney, D. L., Bell, J. F., Vilas, F., 2006. Detection
879 and discrimination of sulfate minerals using reflectance spectroscopy. *Icarus* 184, 121-
880 157.
- 881 Dumke, A., Spiegel, M., van Gasselt, S., Neu, D., Neukum, G., 2010, Systematic Processing of
882 High-Resolution Digital Terrain Model Quadrangles on the Basis of Mars-Express HRSC
883 Data. *Lunar Planet. Sci.* 41, 1980.
- 884 Gendrin, A., Mangold, N., Bibring, J.-P., Langevin, Y., Gondet, B., Poulet, F., Bonello, G.,
885 Quantin, C., Mustard, J., Arvidson, R., LeMouélic, S., 2005. Sulfates in Martian Layered
886 Terrains: The OMEGA/Mars Express View. *Science* 307, 5715, 1587-1591.

- 887 Glotch, T. D., Rogers, A. D., 2007. Evidence for aqueous deposition of hematite- and sulfate-
888 rich light-toned layered deposits in Aureum and Iani Chaos, Mars. *J. Geophys. Res.*
889 (Planets) 112, E6, 06001.
- 890 Gwinner, K., Hauber, E., Jaumann, R., Neukum, G., 2000. High-resolution, digital
891 photogrammetric mapping: A tool for Earth science. *EOS Transactions* 81, 513-513.
- 892 Harrison, K. P., Chapman, M. G., 2008. Evidence for ponding and catastrophic floods in central
893 Valles Marineris, Mars. *Icarus* 198, 351-364.
- 894 Höller, H., 1967. Experimentelle Bildung von Alunit-Jarosit durch die Einwirkung von
895 Schwefelsäure auf Mineralien und Gesteine. *Contrib. Mineral. Petrol.* 15, 4, 309-329.
- 896 Kneissl, T., van Gasselt, S., Neukum, G., 2010. Measurement of Strike and Dip of Geologic
897 Layers from Remote Sensing Data - New Software Tool for ArcGIS. *Lunar Planet. Sci.*
898 41, 1640.
- 899 Komatsu, G., Geissler, P. E., Strom, R. G., Singer, R. B., 1993. Stratigraphy and erosional
900 landforms of layered deposits in Valles Marineris, Mars. *J. Geophys. Res.* 98, E6, 11105
901 - 11121.
- 902 Le Deit, L., Bourgeois, O., Mège, D., Hauber, E., Le Mouélic, S., Massé, M., Jaumann, R.,
903 Bibring, J. P., 2010. Morphology, stratigraphy, and mineralogical composition of a
904 layered formation covering the plateaus around Valles Marineris, Mars: Implications for
905 its geological history. *Icarus* 208, 684-703.
- 906 Le Deit, L., Le Mouélic, S., Bourgeois, O., Combe, J.-P., Mège, D., Sotin, C., Gendrin, A.,
907 Hauber, E., Mangold, N., Bibring, J.-P., 2008. Ferric oxides in East Candor Chasma,
908 Valles Marineris (Mars) inferred from analysis of OMEGA/Mars Express data:
909 Identification and geological interpretation. *J. Geophys. Res. (Planets)* 113, 07001.
- 910 LeDeit, L., 2008. Les dépôts stratifiés dans la région de Valles Marineris (Mars): composition
911 minéralogique et morphologie. *Faculté de Sciences et des Techniques. Université de*
912 *Nantes, Nantes*, 288.
- 913 Lichtenberg, K. A., Arvidson, R. E., Morris, R. V., Murchie, S. L., Bishop, J. L., Fernandez
914 Remolar, D., Glotch, T. D., Noe Dobrea, E., Mustard, J. F., Andrews-Hanna, J., Roach,
915 L. H., 2010. Stratigraphy of hydrated sulfates in the sedimentary deposits of Aram Chaos,
916 Mars. *J. Geophys. Res.* 115, E00D17.
- 917 Loizeau, D., Mangold, N., Poulet, F., Bibring, J. P., Gendrin, A., Ansan, V., Gomez, C., Gondet,
918 B., Langevin, Y., Masson, P., Neukum, G., 2007. Phyllosilicates in the Mawrth Vallis
919 region of Mars. *J. Geophys. Res. (Planets)* 112, E8.
- 920 Lucchitta, B. K., 1987. Valles Marineris, Mars - Wet debris flows and ground ice. *Icarus* 72,
921 411-429.
- 922 Lucchitta, B. K., 1999. Geologic Map of Ophir and Central Candor Chasmata (MTM -5072) of
923 Mars. U. S. Geological Survey,
- 924 Lucchitta, B. K., 2002. Late Mafic Volcanism in Valles Marineris, Mars. *Lunar Planet. Sci.* 40,
925 1636.
- 926 Lucchitta, B. K., 2009a, Lakes in Valles Marineris, Mars (I): Walls, Mounds, Moats, and
927 Volcanoes. *Lunar Planet. Sci.* 40, 2068.
- 928 Lucchitta, B. K., 2009b, Lakes in Valles Marineris, Mars (II): Valleys, Channels, Shallow Lakes,
929 and Age. *Lunar Planet. Sci.*, 2345.
- 930 Lucchitta, B. K., McEwen, A. S., Clow, G. D., Geissler, P. E., Singer, R. B., Schultz, R. A.,
931 Squyres, S. W., 1992. The canyon system on Mars. *Mars*, pp. 453-492.

- 932 Madden, M. E., Bodnar, R. J., Rimstidt, J. D., 2004. Jarosite as an indicator of water-limited
933 chemical weathering on Mars. *Nature* 431, 821-823.
- 934 Malin, M. C., Bell, J. F., Cantor, B. A., Caplinger, M. A., Calvin, W. M., Clancy, R. T., Edgett,
935 K. S., Edwards, L., Haberle, R. M., James, P. B., Lee, S. W., Ravine, M. A., Thomas, P.
936 C., Wolff, M. J., 2007. Context Camera Investigation on board the Mars Reconnaissance
937 Orbiter. *J. Geophys. Res. (Planets)* 112, E5.
- 938 Malin, M. C., Danielson, G. E., Ingersoll, A. P., Masursky, H., Veverka, J., Ravine, M. A.,
939 Soulanille, T. A., 1992. Mars Observer camera. *J. Geophys. Res.* 97, 7699-7718.
- 940 Malin, M. C., Edgett, K. S., 2000. Sedimentary Rocks of Early Mars. *Science* 290, 5498, 1927 -
941 1937.
- 942 Mangold, N., Gendrin, A., Gondet, B., Lemouelic, S., Quantin, C., Ansan, V., Bibring, J.-P.,
943 Langevin, Y., Masson, P., Neukum, G., 2008. Spectral and geological study of the
944 sulfate-rich region of West Candor Chasma, Mars. *Icarus* 194, 519-543.
- 945 Mangold, N., Gendrin, A., Quantin, C., Bibring, J. P., Gondet, B., Langevin, Y., Poulet, F.,
946 Arvidson, R., Griffes, J. L., Hauber, H., Masson, P., Neukum, G., Omega, T., Team, H.
947 C.-I., 2007. An Overview of the Sulfates Detected in the Equatorial Regions by the
948 OMEGA/MEx Spectrometer. *LPI Contributions* 1353, 3141.
- 949 McCord, T. B., Adams, J. B., Bellucci, G., Combe, J. P., Gillespie, A. R., Hansen, G., Hoffmann,
950 H., Jaumann, R., Neukum, G., Pinet, P., Poulet, F., Stephan, K., 2007. Mars Express High
951 Resolution Stereo Camera spectrophotometric data: Characteristics and science analysis.
952 *J. Geophys. Res. (Planets)* 112, E6.
- 953 McCubbin, F. M., Tosca, N. J., Smirnov, A., Nekvasil, H., Steele, A., Fries, M., Lindsley, D. H.,
954 2009. Hydrothermal jarosite and hematite in a pyroxene-hosted melt inclusion in martian
955 meteorite Miller Range (MIL) 03346: Implications for magmatic-hydrothermal fluids on
956 Mars. *Geochim. Cosmochim. Acta* 73, 4907-4917.
- 957 McEwen, A. S., Eliason, E. M., Bergstrom, J. W., Bridges, N. T., Hansen, C. J., Delamere, W.
958 A., Grant, J. A., Gulick, V. C., Herkenhoff, K. E., Keszthelyi, L., Kirk, R. L., Mellon, M.
959 T., Squyres, S. W., Thomas, N., Weitz, C. M., 2007. Mars Reconnaissance Orbiter's High
960 Resolution Imaging Science Experiment (HiRISE). *J. Geophys. Res. (Planets)* 112, E5.
- 961 McGuire, P. C., Bishop, J. L., Brown, A. J., Fraeman, A. A., Marzo, G. A., Frank Morgan, M.,
962 Murchie, S. L., Mustard, J. F., Parente, M., Pelkey, S. M., Roush, T. L., Seelos, F. P.,
963 Smith, M. D., Wendt, L., Wolff, M. J., 2009. An improvement to the volcano-scan
964 algorithm for atmospheric correction of CRISM and OMEGA spectral data. *Planet. Space*
965 *Sci.* 57, 809-815.
- 966 McKay, C. P., Nedell, S. S., 1988. Are there carbonate deposits in the Valles Marineris, Mars?
967 *Icarus* 73, Jan. 1988, 142-148.
- 968 Mège, D., Bourgeois, O., 2010. Destabilization of Valles Marineris Wallslopes by Retreat of
969 Ancient Glaciers. *Lunar Planet. Sci.* 41, 1713.
- 970 Metz, J. M., Grotzinger, J. P., Mohrig, D., Milliken, R., Prather, B., Pirmez, C., McEwen, A. S.,
971 Weitz, C. M., 2009. Sublacustrine depositional fans in southwest Melas Chasma. *J.*
972 *Geophys. Res. (Planets)* 114, 10002.
- 973 Milliken, R. E., Swayze, G., Arvidson, R. E., Bishop, J. L., Clark, R. N., Ehlmann, B. L.,
974 Grotzinger, J., Morris, R. V., Murchie, S. L., Mustard, J. F., Weitz, C. M., Team, C. S.,
975 2008. Spectral Evidence for Sedimentary Silica on Mars. *Lunar Planet. Sci.* 39, 2025.
- 976 Moehlmann, D. T. F., Niemand, M., Formisano, V., Savijärvi, H., Wolkenberg, P., 2009. Fog
977 phenomena on Mars. *Planet. Space Sci.* 57, 1987-1992.

- 978 Murchie, S., Arvidson, R., Bedini, P., Beisser, K., Bibring, J. P., Bishop, J., Boldt, J., Cavender,
979 P., Choo, T., Clancy, R. T., Darlington, E. H., Des Marais, D., Espiritu, R., Fort, D.,
980 Green, R., Guinness, E., Hayes, J., Hash, C., Heffernan, K., Hemmler, J., Heyler, G.,
981 Humm, D., Hutcheson, J., Izenberg, N., Lee, R., Lees, J., Lohr, D., Malaret, E., Martin,
982 T., McGovern, J. A., McGuire, P., Morris, R., Mustard, J., Pelkey, S., Rhodes, E.,
983 Robinson, M., Roush, T., Schaefer, E., Seagrave, G., Seelos, F., Silverglate, P., Slavney,
984 S., Smith, M., Shyong, W. J., Strohbahn, K., Taylor, H., Thompson, P., Tossman, B.,
985 Wirzburger, M., Wolff, M., 2007. Compact Reconnaissance Imaging Spectrometer for
986 Mars (CRISM) on Mars Reconnaissance Orbiter (MRO). *J. Geophys. Res. (Planets)* 112,
987 E5.
- 988 Murchie, S., Roach, L., Seelos, F., Milliken, R., Mustard, J., Arvidson, R., Wiseman, S.,
989 Lichtenberg, K., Andrews-Hanna, J., Bishop, J., Bibring, J.-P., Parente, M., Morris, R.,
990 2009a. Evidence for the origin of layered deposits in Candor Chasma, Mars, from mineral
991 composition and hydrologic modeling. *J. Geophys. Res. (Planets)* 114, E12.
- 992 Murchie, S. L., Mustard, J. F., Ehlmann, B. L., Milliken, R. E., Bishop, J. L., McKeown, N. K.,
993 Noe Dobrea, E. Z., Seelos, F. P., Buczkowski, D. L., Wiseman, S. M., Arvidson, R. E.,
994 Wray, J. J., Swayze, G., Clark, R. N., Des Marais, D. J., McEwen, A. S., Bibring, J.-P.,
995 2009b. A synthesis of Martian aqueous mineralogy after 1 Mars year of observations
996 from the Mars Reconnaissance Orbiter. *J. Geophys. Res.* 114.
- 997 Murchie, S. L., Seelos, F. P., Hash, C. D., Humm, D. C., Malaret, E., McGovern, J. A., Choo, T.
998 H., Seelos, K. D., Buczkowski, D. L., Morgan, M. F., Barnouin-Jha, O. S., Nair, H.,
999 Taylor, H. W., Patterson, G. W., Harvel, C. A., Mustard, J. F., Arvidson, R. E., McGuire,
1000 P., Smith, M. D., Wolff, M. J., Titus, T. N., Bibring, J.-P., Poulet, F., 2009c. Compact
1001 Reconnaissance Imaging Spectrometer for Mars investigation and data set from the Mars
1002 Reconnaissance Orbiter's primary science phase. *J. Geophys. Res.* 114, E00D07.
- 1003 Nedell, S. S., Squyres, S. W., Andersen, D. W., 1987. Origin and evolution of the layered
1004 deposits in the Valles Marineris, Mars. *Icarus* 70, June 1987, 409-441.
- 1005 Neukum, G., Jaumann, R., 2004. HRSC: the High Resolution Stereo Camera of Mars Express.
1006 *Mars Express: the Scientific Payload*, 17-35.
- 1007 Papike, J. J., Karner, J. M., Shearer, C. K., 2006. Comparative planetary mineralogy:
1008 Implications of martian and terrestrial jarosite. A crystal chemical perspective. *Geochim.*
1009 *Cosmochim. Acta* 70, 1309-1321.
- 1010 Parente, M., 2008. A New Approach to Denoising CRISM Images. *Lunar Planet. Sci.*, 2528.
- 1011 Pelkey, S. M., Mustard, J. F., Murchie, S., Clancy, R. T., Wolff, M., Smith, M., Milliken, R.,
1012 Bibring, J. P., Gendrin, A., Poulet, F., Langevin, Y., Gondet, B., 2007. CRISM
1013 multispectral summary products: Parameterizing mineral diversity on Mars from
1014 reflectance. *J. Geophys. Res. (Planets)* 112, E8.
- 1015 Peterson, C. M., 1981. Hebes Chasma - Martian Pyroclastic Sink. *Lunar Planet. Sci.*, 828-829.
- 1016 Poulet, F., Arvidson, R. E., Gomez, C., Morris, R. V., Bibring, J. P., Langevin, Y., Gondet, B.,
1017 Griffes, J., 2008. Mineralogy of Terra Meridiani and western Arabia Terra from
1018 OMEGA/MEx and implications for their formation. *Icarus* 195, 106-130.
- 1019 Quantin, C., Allemand, P., Mangold, N., Delacourt, C., 2004. Ages of Valles Marineris (Mars)
1020 landslides and implications for canyon history. *Icarus* 172, 555-572.
- 1021 Quantin, C., Mangold, N., Hauber, E., Flahaut, J., Le Deit, L., Fueten, F., Zegers, T., 2010.
1022 Timing Constrains of Interior Layered Deposit Emplacement in Valles Marineris. First
1023 International Conference on Mars Sedimentology and Stratigraphy, 53.

- 1024 Roach, L. H., 2009, Sulfates in Valles Marineris as Indicators of the Aqueous Evolution of Mars.
1025 Department of Geological Sciences. Brown University, Providence, RI 296.
- 1026 Roach, L. H., Mustard, J. F., Lane, M. D., Bishop, J. L., Murchie, S. L., 2010a. Diagenetic
1027 haematite and sulfate assemblages in Valles Marineris. *Icarus* 207, 659-674.
- 1028 Roach, L. H., Mustard, J. F., Swayze, G., Milliken, R. E., Bishop, J. L., Murchie, S. L.,
1029 Lichtenberg, K., 2010b. Hydrated mineral stratigraphy of Ius Chasma, Valles Marineris.
1030 *Icarus* 206, 253-268.
- 1031 Rossi, A. P., Neukum, G., Pondrelli, M., van Gasselt, S., Zegers, T., Hauber, E., Chicarro, A.,
1032 Foing, B., 2008. Large-scale spring deposits on Mars? *J. Geophys. Res. (Planets)* 113,
1033 E8.
- 1034 Sánchez España, J., López Pamo, E., Santofimia, E., Aduvire, O., Reyes, J., Baretino, D., 2005.
1035 Acid mine drainage in the Iberian Pyrite Belt (Odiel river watershed, Huelva, SW Spain):
1036 Geochemistry, mineralogy and environmental implications. *Appl. Geochem.* 20, 7, 1320-
1037 1356.
- 1038 Schiffman, P., Zierenberg, R., Marks, N., Bishop, J. L., Darby Dyar, M., 2006. Acid-fog
1039 deposition at Kilauea volcano: A possible mechanism for the formation of siliceous-
1040 sulfate rock coatings on Mars. *Geology* 34, 921.
- 1041 Sherman, D. M., Burns, R. G., Mee Burns, V., 1982. Spectral characteristics of the iron oxides
1042 with application to the Martian bright region mineralogy. *J. Geophys. Res.* 87, 10169-
1043 10180.
- 1044 Sunshine, J. M., Pieters, C. M., 1990, Extraction of Compositional Information from Olivine
1045 Reflectance Spectra: A New Capability for Lunar Exploration. *Lunar Planet. Sci.* 30,
1046 1223.
- 1047 Tosca, N. J., Milliken, R. E., Michel, F. M., 2008. Smectite Formation on Early Mars:
1048 Experimental Constraints. *LPI Contributions* 1441, 77-78.
- 1049 Triantafyllidis, S., Skarpelis, N., 2006. Mineral formation in an acid pit lake from a high-
1050 sulfidation ore deposit: Kirki, NE Greece. *J. Geochem. Explor.* 88, 1-3, 68-71.
- 1051 Weitz, C. M., Lane, M. D., Staid, M., Dobrea, E. N., 2008. Gray hematite distribution and
1052 formation in Ophir and Candor chasmata. *J. Geophys. Res. (Planets)* 113, 02016.
- 1053 Williams, D. A., Greeley, R., Ferguson, R. L., Kuzmin, R., McCord, T. B., Combe, J.-P., Head,
1054 J. W., Xiao, L., Manfredi, L., Poulet, F. o., Pinet, P., Baratoux, D., Plaut, J. J., Raitala, J.,
1055 Neukum, G., the, H. C.-I. T., 2009. The Circum-Hellas Volcanic Province, Mars:
1056 Overview. *Planet. Space Sci.* 57, 895-916.
- 1057 Zegers, T. E., Dabekaussen, W., Hauber, E., Gwinner, K., Scholten, F., Fueten, F., Stesky, R.,
1058 MacKinnon, P., Neukum, G., Team, H. C.-I., 2006, 3D Structural Analysis of Ophir
1059 Chasma Based on HRSC Image Data and Stereo-derived DTM. *Lunar and Planet. Sci.*
1060 36, 1605.
- 1061 Zorzano, M. P., Mateo-Martí, E., Prieto-Ballesteros, O., Osuna, S., Renno, N., 2009. Stability of
1062 liquid saline water on present day Mars. *Geophys. Res. Lett.* 36.
1063
1064
1065

1066 [TABLES]

1067

1068

1069

1070 **Table 1:** List of CRISM and OMEGA observations used in this study

CRISM targeted observations ^a	CRISM Multispectral Mapping Strips ^a	OMEGA observations ^b
FRT000082C5_07	MSP000031C3_05	0548_3
FRT000096E6_07	MSP000032FE_05	1180_5
FRT0000A86A_07	MSP000033F3_07	1202_1
FRT0000AD8D_07	MSP000034E0_05	1213_2
FRT0000B27B_07	MSP00003899_01	3228_3
FRT0000B994_07	MSP00003A47_01	4358_3
FRT0000BB63_07	MSP00003EA9_05	4380_3
FRT000109E5_07	MSP00004044_07	
HRL0000508A_07	MSP0000416B_05	
HRL00005B82_07	MSP000046F2_07	
HRL00007468_07	MSP00004825_01	
HRL000075E7_07	MSP00004AA1_01	
HRL00007E21_07	MSP00005575_03	
HRL0000A432_07	MSP000059A0_05	
HRL0000B7D4_07	MSP00006CCB_01	
HRL0000BF5E_07	MSP0000CB50_01	
HRL0000C30D_07		
HRL0000C59C_07		

1071 ^aThe first three characters of the CRISM file names designate the type of observation: full(FRT) or half resolution
 1072 targeted (HRL) observation or multispectral mapping strip (MSP). The next characters are unique hexadecimal
 1073 identifiers for each observation. The last two figures indicate the component image used from that observation.

1074 ^b OMEGA observations are identified by the four-digit orbit number followed by the sequence number within that
 1075 orbit

1076

1077 [FIGURE CAPTIONS]

1078

1079 Figure 1

1080 A: Color mosaic of HRSC orbits 334 and 3127 of Ophir Chasma with location names and
1081 simplified geologic units. Contour lines every 500 m from HRSC DTM with 150 m post spacing.

1082 Dashed red line: Prominent marker horizon in Ophir Mensa, separating it in a lower and upper

1083 unit. Local layer strike and dip measurements. Compare to Zegers et al., 2006.

1084 B: HRSC nadir mosaic with contour lines for orientation, overlain with 'ratio of reflectance at 1

1085 and 1.3 μm ', SINDEX and BD2100 as RGB image from OMEGA and CRISM multispectral and

1086 targeted observations, and resulting mineralogic units (white lines). Iron oxides appear red,

1087 polyhydrated sulfates green, monohydrated sulfates blue.

1088

1089 Figure 2

1090 Details of the horizon marked red in Fig. 1. In the west of Ophir Mensa, it forms a steep cliff

1091 near the top of the mound (A). In the center of Ophir Mensa, it plunges at angles around 4° under

1092 the overlying LTDs further east and north (B). CTX images P02_002208_1748,

1093 P12_005676_1746, P15_006955_1746.

1094

1095 Figure 3

1096 A: CTX observation P20_008893_1762 from western Ophir Mensa, overlain with spectral

1097 indices from CRISM FRT0000B27B as in Fig. 1, showing presence of kieserite (blue) and a

1098 weak presence of polyhydrated sulfates (green). The red stripe is an artifact.

1099 B: Detail of HiRISE observation PSP_008458_1760. MHS: monohydrated sulfates. The kieserite

1100 detection boundary is controlled by dust cover and oblique to layering, suggesting that kieserite

1101 is abundant in this part of Ophir Mensa despite spatially limited detections, whereas the area
1102 showing the PHS signature is stronger affected by dust.

1103
1104 Figure 4

1105 A: HRSC orbit 334 of the "mineral bowl" overlain with HRSC contours and spectral indices as
1106 in fig. 1. Red dashed line: Prominent horizon in Ophir Mensa. Sulfate detections are restricted to
1107 units below this horizon.

1108 B: Interpreted mineralogic map of same region. MHS: monohydrated sulfates. PHS:
1109 Polyhydrated sulfates.

1110
1111 Figure 5

1112 A: Detail of fig 4 showing the complex stratigraphic relationship between Ophir Mensa, LTDs
1113 on southern chasm wall and basaltic wall rock (CTX P12_005676_1746 and P13_006243_1746
1114 overlain on HRSC color image orbit 3127) North is left. Mineralogy as in Fig. 4, combined with
1115 geomorphologic interpretation. MHS: monohydrated sulfates. PHS: polyhydrated sulfates. White
1116 arrow: Light-toned material on ridge of southern wall. Black arrow: "Tongue" of LTD bridging a
1117 valley between Ophir Mensa and southern wall. This implies that a depression already existed at
1118 this location at the time of sulfate deposition (see text). B: Anaglyph from HRSC orbit 3127 of
1119 the same area.

1120 Figure 6

1121 A: CTX observation P03_002208_1748 and P12_005676_1746 of LTDs on southern chasm wall
1122 overlain with spectral indices from FRT0000A86A as in fig. 1. Contours from HRSC DTM.
1123 LTDs form deposits on top of basaltic wall rock. Layered kieserite is superposed by
1124 polyhydrated sulfates and iron oxides. Layers dip downslope. At base of slope, polyhydrated

1125 sulfates embay kieserite, suggesting discordant deposition. B: Same as A, but spectral indices
1126 BD2210, BD2230 and ratio between reflectance at 2.33 μm and 2.28 μm as red, green and blue
1127 color planes. C: locations, where average spectra were taken. Spectra were averaged over tens to
1128 thousands of pixels to reduce noise, and divided by a spectrally inconspicuous reference region
1129 (black). D: Average reflectance spectra of monohydrated sulfates, polyhydrated sulfates, iron
1130 oxides and reference. E: Same spectra as D, ratioed to reflectance spectrum, and matching library
1131 spectra from RELAB. F: Average reflectance spectra of the three spectrally distinct regions in B,
1132 in the range of 0.41 μm to 2.6 μm , together with ferric oxide spectrum and reference for
1133 comparison. Three phases are observed: A phase with absorption band at 2.21 μm (magenta),
1134 one with a band at 2.23 μm (green) jarosite (cyan). G: Ratioed reflectance spectra in the range of
1135 0.41 to 0.64 μm and 0.69 to 0.97 μm with separately removed continuum, and resembling
1136 laboratory spectra. H: Same spectra as in F and G (except ferric oxide), in the spectral range 1 -
1137 2.6 μm , ratioed to reference region spectrum. Spectra resemble jarosite/H₃O-jarosite mixed with
1138 amorphous silica or Al-rich clays (montmorillonite). Library spectra from RELAB, except H₃O-
1139 jarosite from Milliken et al., 2008.

1140

1141 Figure 7

1142 A: Details of LTD at the foot of southern chasm wall (HiRISE anaglyph of ESP_011662_1750
1143 and ESP_011807_1750). B: Detail of ridge in Fig. 6. The 2.21-micron-phase overlays kieserite
1144 as a thin, very bright coating. Its occurrence is restricted to the talus deposit underneath fresh
1145 basaltic ridge. A water supply to this location from groundwater or by a lake is inconsistent.
1146 Instead, water might have precipitated as rain, frost or snow from above. (HiRISE
1147 ESP_011807_1750_COLOR). C: Interpretative cross-sections to A and B (not to scale). The

1148 2.21- μm -phase, the 2.23- μm -phase and the polyhydrated sulfates are found in similar positions
1149 discordantly superposing MHS. The relationship among these phases is unclear due to basaltic
1150 cover. Ferric oxides are found in association with PHS.

1151
1152 Figure 8
1153 Outcrops of light-toned material underneath landslide deposit cover in "northern moat". A and B:
1154 Sulfate-free LTDs at elevations of 3100 and 3300 m below datum.
1155 C: Sulfate-bearing LTD at elevation -4600 m. Possible floor of "northern moat" prior to
1156 landslides. (CTX images P12_005676_1746, P03_002208_1748, P18_007891_1742; contours:
1157 HRSC).

1158
1159 Figure 9
1160 A: Sulfate deposits in landslide superposed on now partly eroded LTD of Ophir Mensa (CTX
1161 P03_002208_1748; spectral indices as in fig. 1).
1162 B: Anaglyph from HRSC orbit 2083 visualizing the stratigraphy. C Interpretative cross-section
1163 of landslide based on HRSC DTM showing sulfates overlaying Ophir Mensa LTD.

1164
1165 Figure 10
1166 A: HRSC nadir (orbit 334) and contours of the central valley of Ophir Chasma overlain with
1167 spectral indices as in fig. 1.
1168 B: HRSC color image with interpreted mineralogy. MHS: Monohydrated sulfates. Polyhydrated
1169 sulfates are found in north of central valley. They are overlain by monohydrated sulfates
1170 (kieserite), iron oxides accumulating in the southern part of the valley, and basaltic dunes.

1171 C: Interpretative longitudinal profile of central valley. Monohydrated sulfates superpose
1172 polyhydrated sulfates.

1173 D: Sulfates are revealed in HRSC color data by their distinct hue.

1174 E: Fluted surface texture of polyhydrated sulfates. (HiRISE PSP_007535_1755_RED)

1175 F: Ridged surface texture of kieserite-bearing valley floor, covered by basaltic dunes (SE of
1176 figure) and iron-oxide rich deposits (SW of figure; CTX P20_008972_1756).

1177 G: Example of curvilinear, sulfate-bearing ridges. Spectral indices from CRISM HRL0000B7D4
1178 as in fig. 1 on HiRISE PSP_009183_1750

1179

1180 Figure 11

1181 A: Spectral index BD2210 of two CRISM HRL observations overlain on CTX images of the
1182 northern central valley (CTX P05_003131_1747, P20_008972_1756), and exemplary spectra.
1183 Spectra resemble jarosite with additional phases mixed in (compare fig. 6).

1184 B and C: Outcrops of the 2.21 μm phase here are subcircular and almost indistinguishable in
1185 texture from the surrounding sulfate-rich rock

1186

1187 Figure 12

1188 Suggested succession of events in Ophir Chasma. 1: Opening of Valles Marineris. 2: Deposition
1189 of the LTDs such as Ophir Mensa, possibly as airfall deposits or ash. 3: Formation of kieserite in
1190 Ophir Mensa by intruding groundwater. 4: Excavation of the "mineral bowl", "central valley"
1191 and "northern moat". 5: Deposition and/or alteration to form polyhydrated sulfates and other
1192 phases in "mineral bowl", possibly by precipitation water. Deposition of PHS and MHS (6) in
1193 "central valley", possibly in lake or underneath a glacier. The relative timing of these events is

1194 not constrained and could coincide with deposition of layered deposits with similar mineralogy
1195 on the plateau above Valles Marineris. 7: Landslides enlarge the chasm and partly cover the
1196 floor.

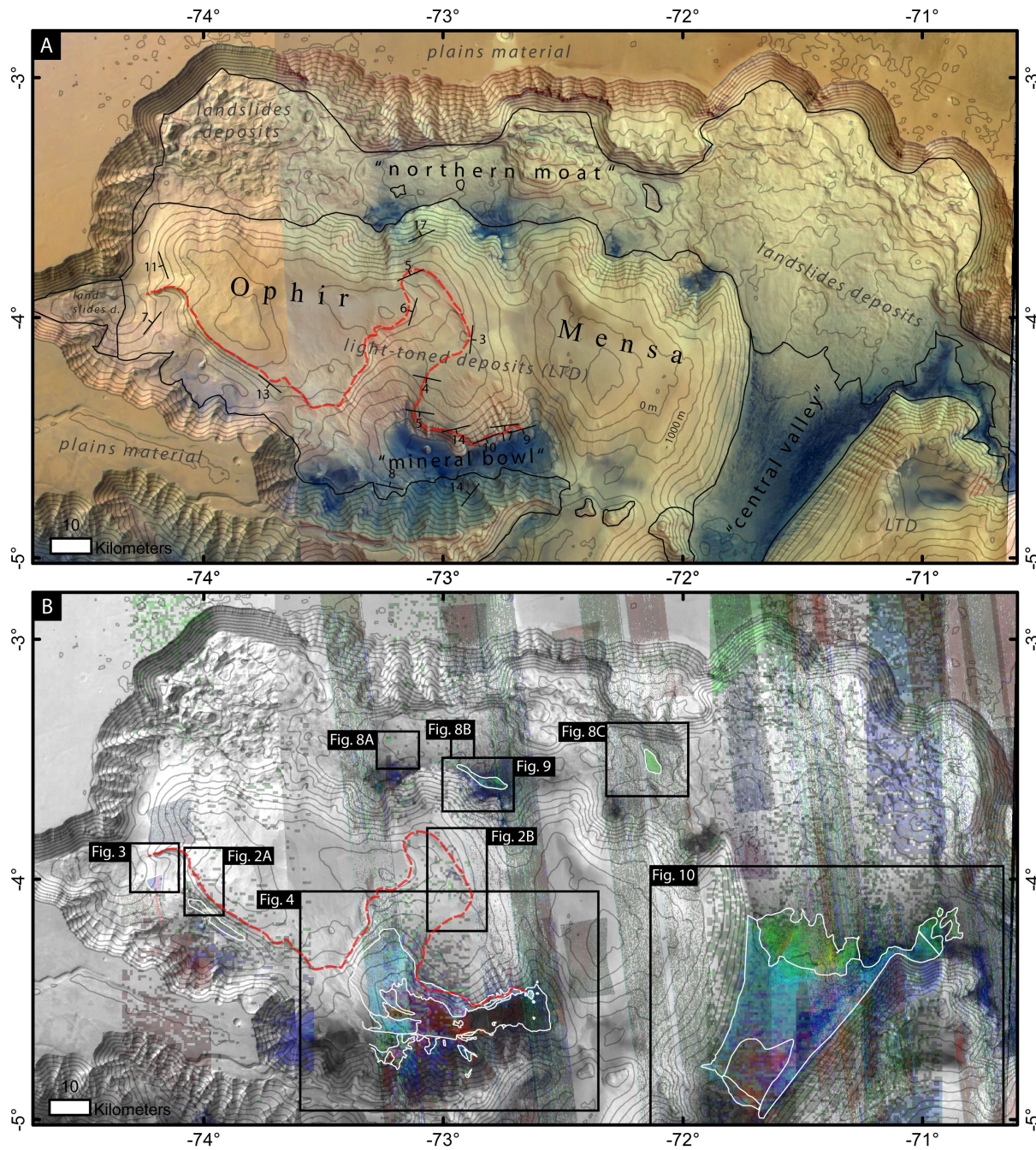
1197

1198

1199 [Figures]

1200 [Figure 1]

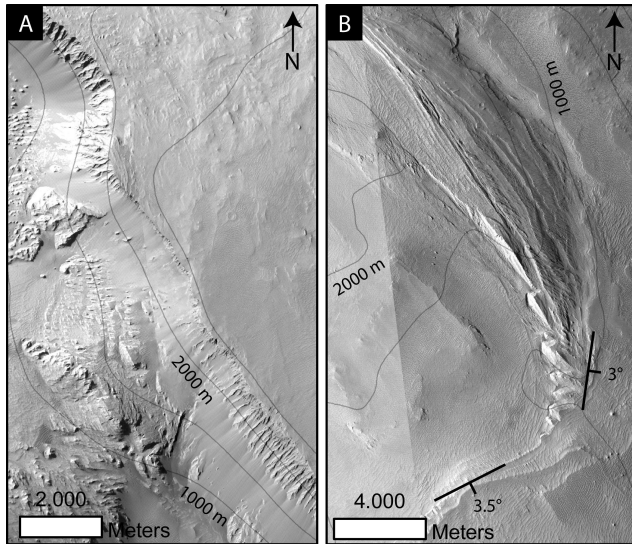
ACCEPTED MANUSCRIPT



1201

1202

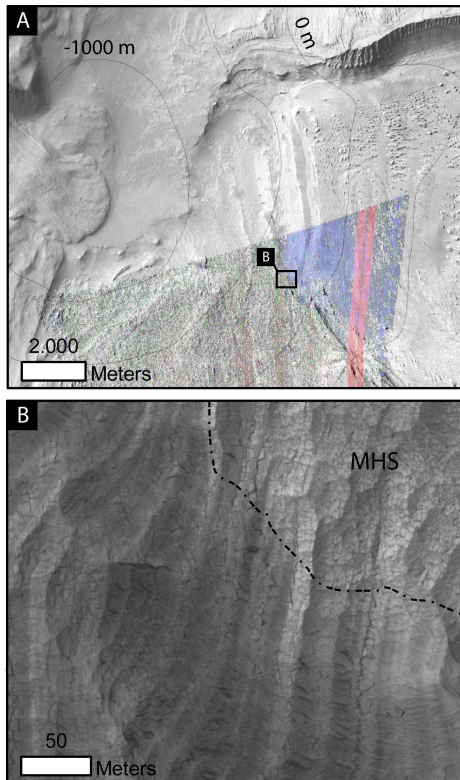
[Figure 2]



1203

1204

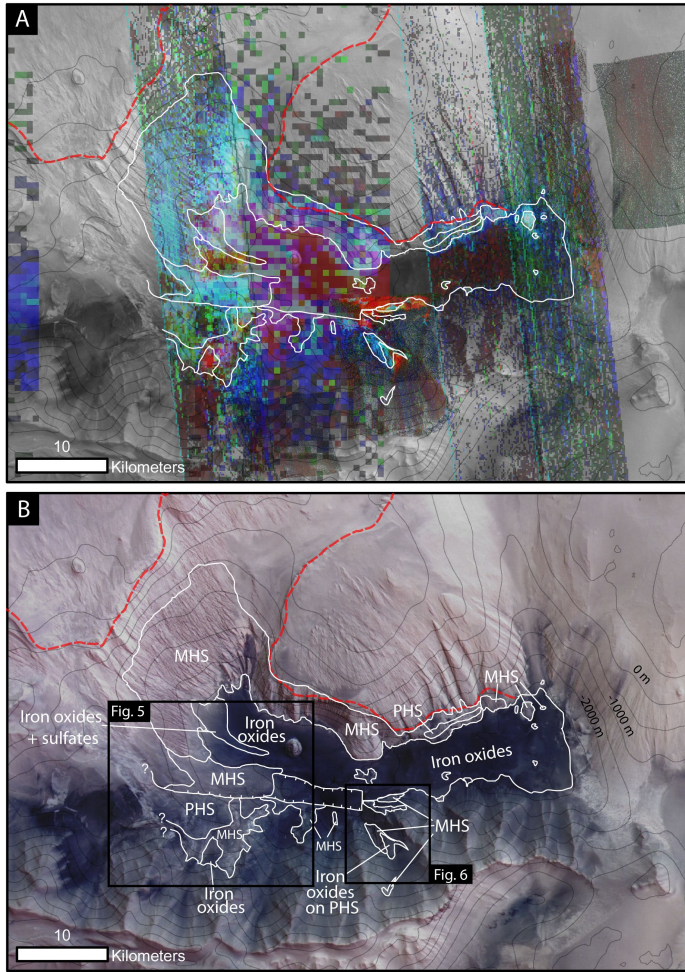
1205 [Figure 3]



1206

1207

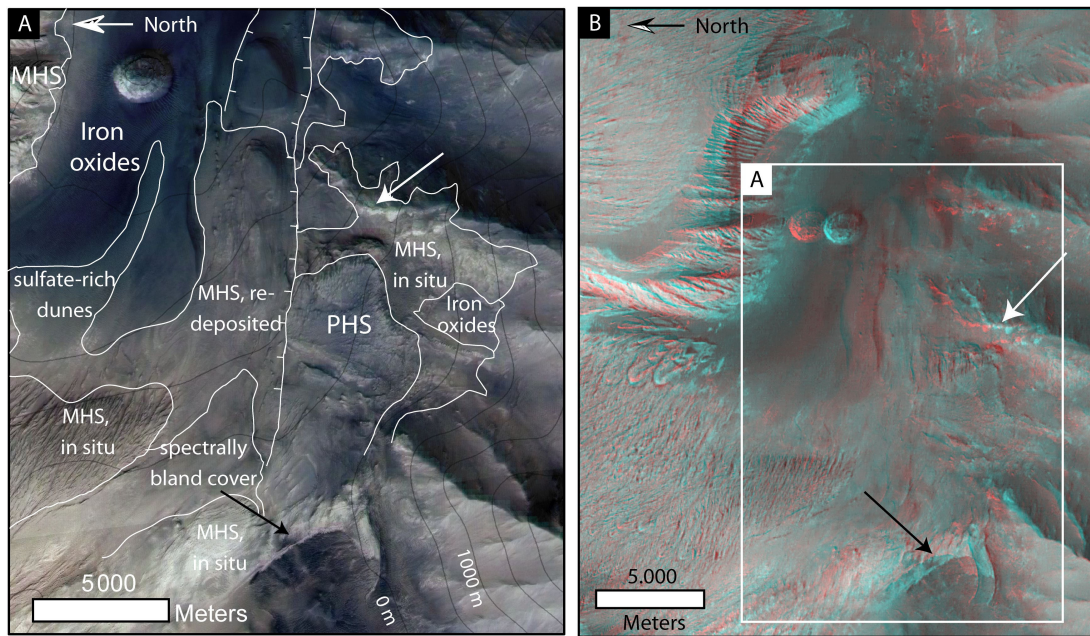
1208 [Figure 4]



1209

1210

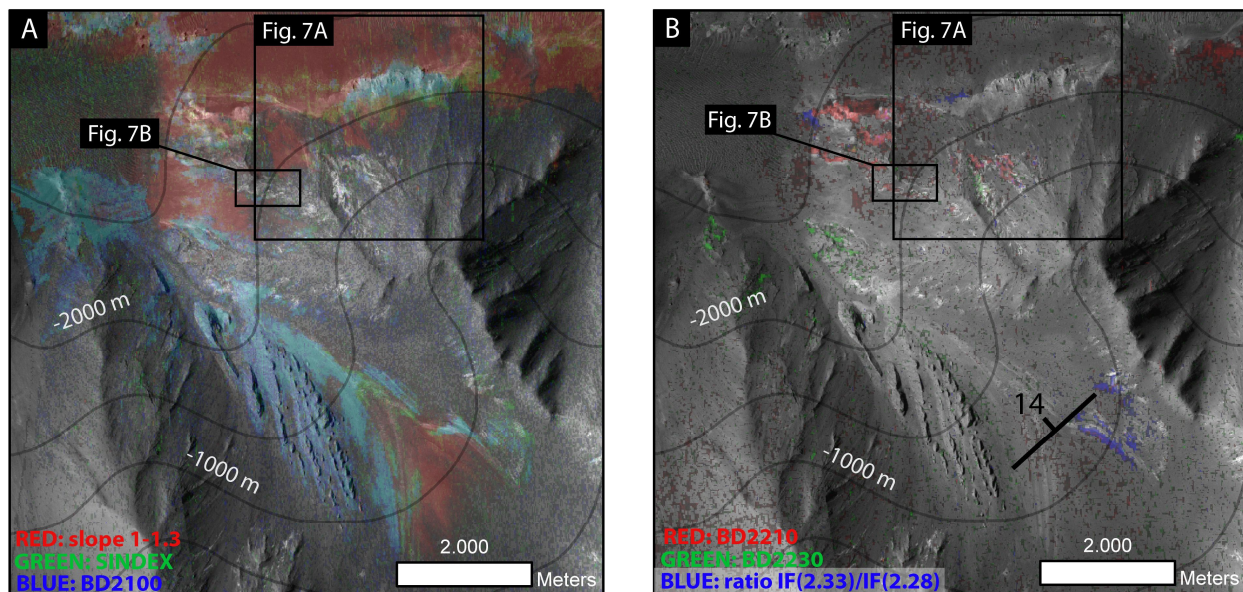
1211 [Figure 5]



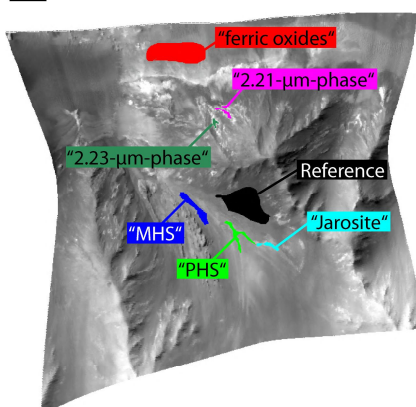
1212

1213 [Figure 6]

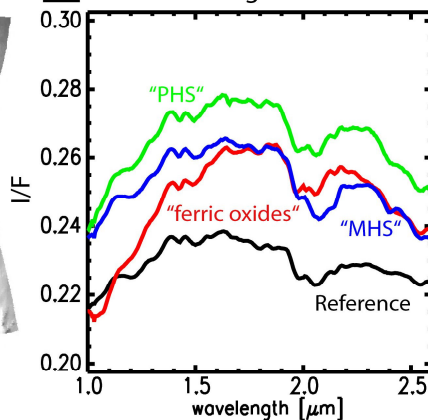
1214



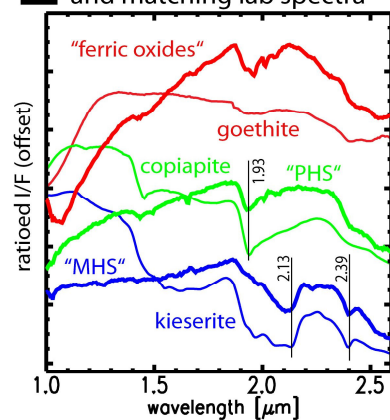
C locations of average spectra



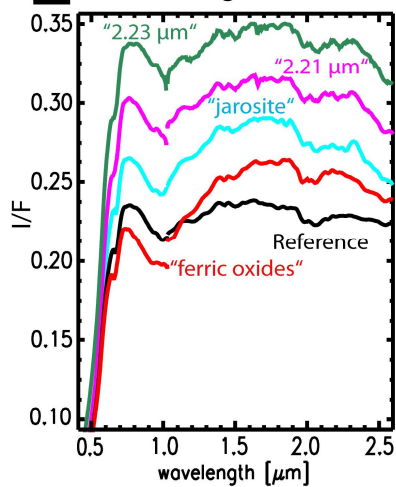
D CRISM average reflectances



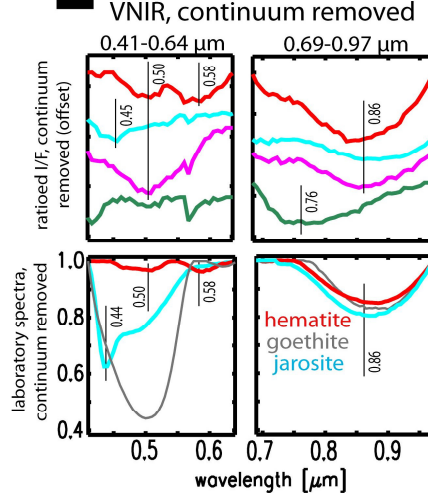
E CRISM ratioed reflectances and matching lab spectra



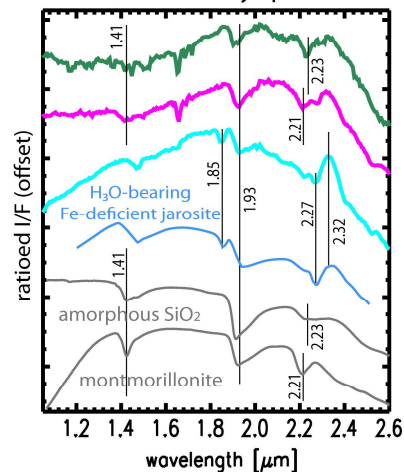
F CRISM average reflectances



G CRISM ratioed reflectances, VNIR, continuum removed



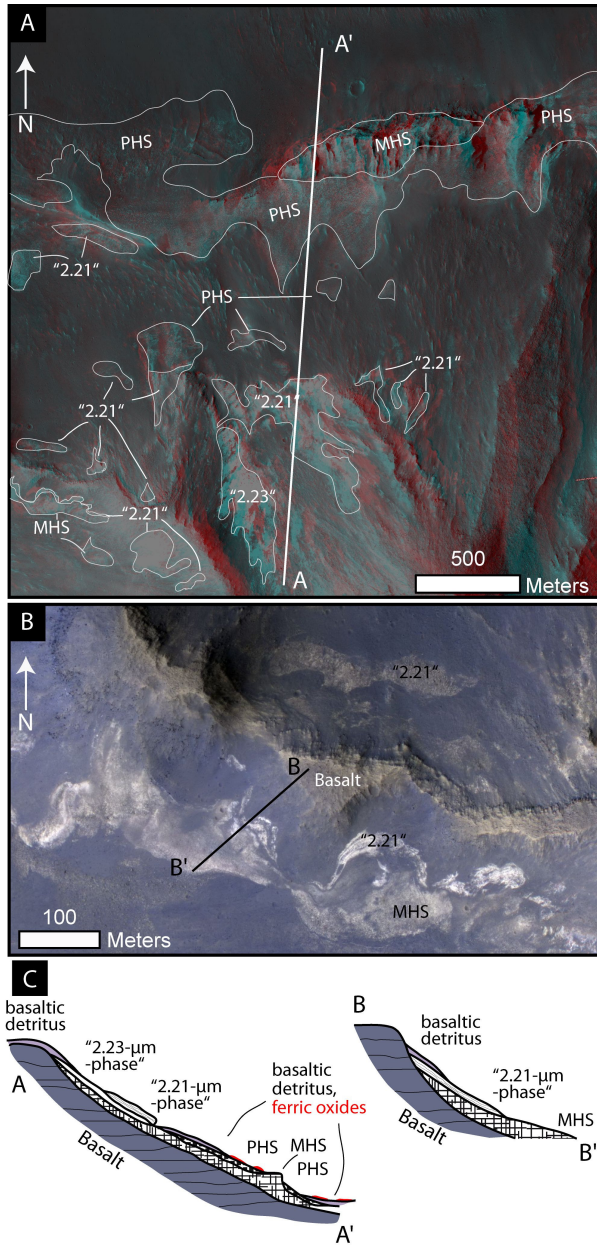
H CRISM ratioed reflectances and laboratory spectra



1215

1216

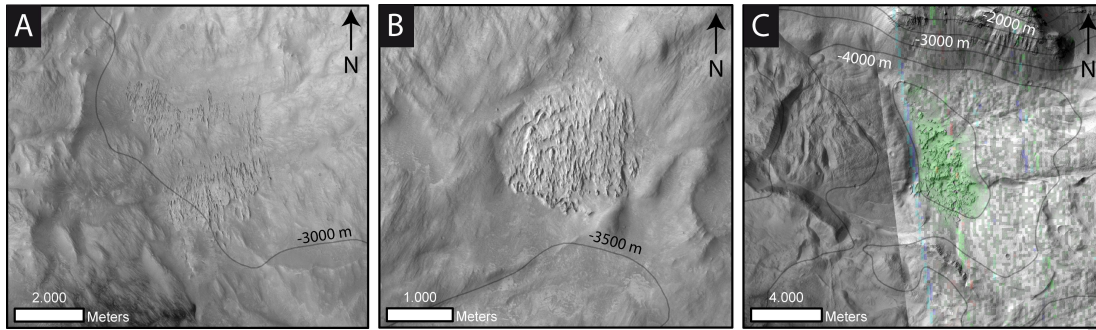
1217 [Figure 7]



1218

1219

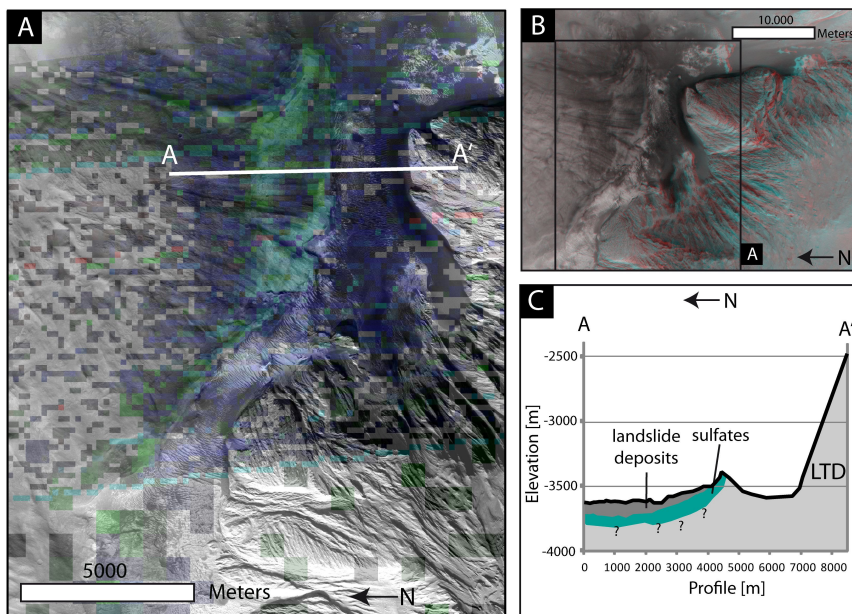
1220 [Figure 8]



1221

1222

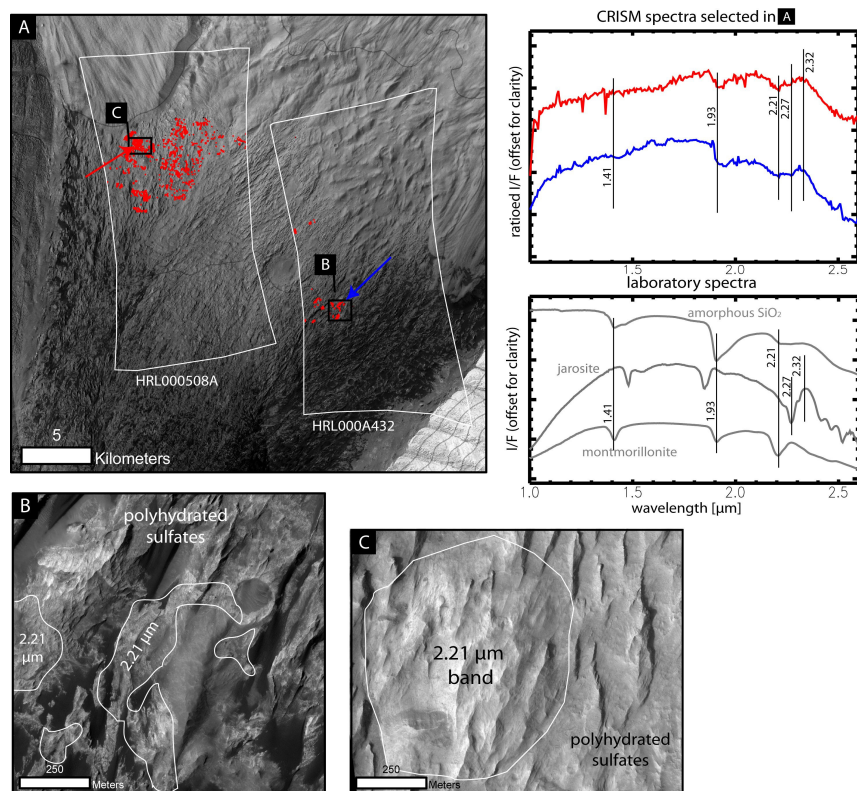
1223 [Figure 9]



1224

1225

1226 [Figure 10]

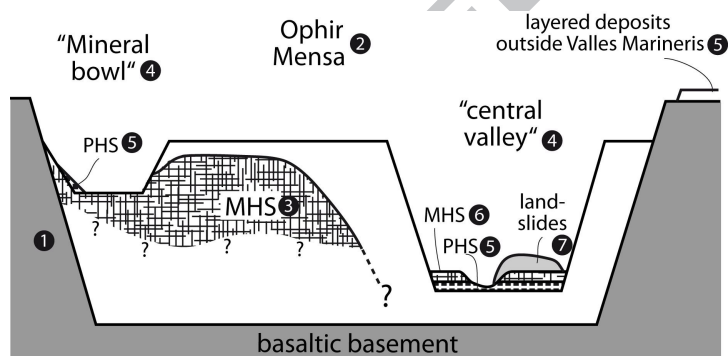


1230

1231

1232 [Figure 12]

1233



Sulfates and Iron Oxides in Ophir Chasma based on OMEGA and CRISM Observations**by Wendt et al.****Research highlights:**

- Detection of jarosite and hydroxylated phases, kieserite, polyhydrated sulfates and hematite
- Interpretation of mineralogy together with digital elevation models and anaglyphs
- Discussion of formation theories
- comparison to light-toned deposits elsewhere on Mars